The Tgf-β family member Gdf6Y determines the male sex in *Nothobranchius furzeri* by suppressing oogenesis-inducing genes

Annekatrin Richter,[1,*] Hanna Mörl,[1] Maria Thielemann,[1,a] Markus Kleemann,[1,b] Raphael Geißen,[1,c] Robert Schwarz,[1] Carolin Albertz,[1] Philipp Koch,[1] Andreas Petzold,[1,d] Marco Groth,[1] Nils Hartmann,[1,e] Amaury Herpin,[2] Christoph Englert[1,3]

[1]Leibniz Institute on Aging – Fritz Lipmann Institute, Jena, Germany

[2]INRAE, LPGP, Rennes, France

[3]Institute of Biochemistry and Biophysics, Friedrich Schiller University Jena, Jena, Germany

[a]Current address: BianoGMP GmbH, Gera, Germany

[b]Current address: Synlab Jena Oncoscreen, Jena, Germany

[c]Current address: Memorial Sloan Kettering Cancer Center, New York, USA

[d]Current address: Technische Universität (TU) Dresden, Dresden, Germany

[e]Current address: Institute of Pathology, University Medical Center Mainz, Mainz, Germany

*Corresponding author: Annekatrin.Richter@leibniz-fli.de

ABSTRACT

The short-lived African killifish *Nothobranchius furzeri* lives in seasonal freshwater ponds and has evolved remarkable traits to survive in this limited environment. One of those traits is a genetic XX/XY sex-determination system, which ensures an equal distribution of both sexes. Comparisons of female and male genomic sequences identified the Y-chromosomal copy of the TGF-β family member *gdf6* as the candidate male sex-determining (SD) gene, which was named *gdf6Y* in contrast to the X-chromosomal allele *gdf6X*. CRISPR/Cas9-mediated inactivation of *gdf6Y* in *N. furzeri* led to a complete male-to-female sex reversal in XY animals. The homozygous inactivation of *gdf6X* on the other hand led to a detrimental phenotype post-hatching. This phenotype was compensated by *gdf6Y*, revealing that the latter became the SD gene while retaining at least some of its original *gdf6* function. *Gdf6Y* is expressed in testicular somatic cells already prior to hatching, where it represses the germ cell-intrinsic feminizing gene *foxl2l.* We have identified components of the TGF-β signaling pathway, especially the inhibitor of DNA binding genes *id1/2/3*, and the mRNA decay activator *zfp36l2*, as Gdf6Y targets. We conclude that Gdf6Y exerts its function as the male sex-determining gene by suppressing female-specific genes in the developing gonad of male *N. furzeri*.

36 **INTRODUCTION**

37 The African turquoise killifish *Nothobranchius furzeri* is the captive vertebrate with the shortest
38 lifespan of about 6 months reported so far (Platzer and Englert 2016). Despite its short lifespan,
39 *N. furzeri* shows remarkable aging phenotypes and, therefore, is an upcoming model organism,
40 especially in aging research (Kim et al. 2016; Reuter et al. 2018). The annual killifish species
41 inhabits ephemeral ponds in the South of Zimbabwe and Mozambique. From several of these
42 isolated wild populations, laboratory strains with varying lifespans and different tail colors were
43 derived e. g., the yellow-tailed strain GRZ with a lifespan of 6 months from Zimbabwe (Jubb 1971)
44 and the strains MZM0403 and MZM0410 with an around 1-year lifespan from Mozambique
45 (Terzibasi et al. 2008; Tozzini et al. 2013). In the wild, the embryos survive the dry season by
46 facultative developmental arrests named diapauses. In direct development without diapause, the
47 embryos enter the pharyngula stage and continue organogenesis at about 9 days post-fertilization
48 (dpf), which is completed at around 14 dpf (Api et al. 2018). Between three and four weeks after
49 fertilization, the embryos are ready to hatch. This so-called hatching stage (0 days post-hatching –
50 0 dph) can be maintained for several weeks. After hatching the larvae quickly grow, reach sexual
51 maturation, and develop a strong sexual dimorphism at three to four weeks post-hatching. With a
52 1:1 sex ratio, males were found to be the heterogametic sex, and an XY sex-determination system
53 was suggested (Valenzano et al. 2009). Only when the species' genome was sequenced, the sex
54 chromosome pair was identified (Reichwald et al. 2015; Valenzano et al. 2015) and the Y-
55 chromosomal copy of the growth differentiation factor 6 gene (*gdf6*), which was therefore named
56 *gdf6Y*, was proposed as the potential sex-determining (SD) gene (Reichwald et al. 2015).

57 Gdf6 is a secreted ligand-protein that belongs to the bone morphogenetic proteins (BMPs), a group
58 of the transforming growth factor beta (TGF-β) superfamily. These proteins consist of an N-

59 terminal prodomain, which is proteolytically cleaved-off upon maturation, and the C-terminal
60 ligand portion, which binds as a dimer to members of the corresponding TGF-β receptor family.
61 This leads to the intracellular activation of receptor-regulated SMAD transcription factors (R-
62 SMADs) by phosphorylation and ultimately regulates gene expression. Other TGF-β ligand and
63 receptor family members, including orthologs of *amh*, *amhrII*, *bmprI*, and *gsdf*, have been
64 previously identified as SD genes in various fish species (Hattori et al. 2012; Kamiya et al. 2012;
65 Myosho et al. 2012; Kikuchi and Hamaguchi 2013; Li et al. 2015; Pan et al. 2019; Feron et al.
66 2020; Peichel et al. 2020; Herpin et al. 2021; Pan et al. 2021; Holborn et al. 2022). Therefore,
67 factors involved in TGF-β signaling constitute one functional group, out of which SD genes are
68 recruited in fishes. The other main group of SD gene candidates is transcription factors, especially
69 those already involved in sex determination like *Dmrt1* and *Sox* genes (Pan et al. 2021). The SD
70 gene of the rainbow trout (*Oncorhynchus mykiss*), *sdY*, is an exception, as its ancestral gene *irf9* is
71 an immune-related transcription factor (Yano et al. 2012).

72 In the sequenced *N. furzeri* strain GRZ, *gdf6Y* differs from the X chromosomal *gdf6* copy, hereafter
73 called *gdf6X*, in 22 single nucleotide polymorphisms (SNPs) and a 9-bp deletion in the coding
74 sequence (CDS) of the prodomain (Fig. 1 A; Supplemental Fig. S1 A; Reichwald et al. (2015)).
75 While the non-synonymous SNPs and the 9-bp deletion are conserved among the laboratory *N.*
76 *furzeri* strains analyzed so far, the size of the genomic region, which accumulated differences
77 between the X and Y chromosome, varies greatly from 196 kb to 37 Mb in the strains MZM0403
78 and MZM0410, respectively, indicating the ongoing evolution of the species' sex chromosomes.
79 In other teleost and tetrapod species, including zebrafish, *Xenopus laevis*, mice, and humans,
80 *GDF6* orthologs were predominantly shown to be involved in joint development and eye formation
81 (Settle et al. 2003; Hanel and Hensey 2006; Asai-Coakwell et al. 2007; Tassabehji et al. 2008;

82 Asai-Coakwell et al. 2009; Gosse and Baier 2009; den Hollander et al. 2010; Reed and Mortlock
83 2010; Asai-Coakwell et al. 2013), but also the involvement in vascularization (Crosier et al. 2002;
84 Hall et al. 2002; Krispin et al. 2018) and melanoma as well as melanocyte development were
85 observed (Venkatesan et al. 2018; Gramann et al. 2019).

86 Here, we demonstrate *gdf6Y* as the SD gene in *N. furzeri* by specifically disrupting the Y-
87 chromosomal allele. The respective mutants showed a complete male-to-female sex reversal. The
88 homozygous inactivation of the X-chromosomal allele *gdf6X* on the other hand led to a detrimental
89 curled tail phenotype, which abolished proper larval swimming immediately after hatching.
90 However, *gdf6Y* compensates for the loss of *gdf6X* and, therefore, must have additionally acquired
91 the SD gene function. In this role, *gdf6Y* is expressed in the male gonad by a subset of somatic
92 cells at 0 dph and in Sertoli cells in adulthood. At 0 dph, however, oogenesis has already begun in
93 the female gonads, and thereby the sex in *N. furzeri* must be determined beforehand. As suggested
94 by the analyses of mutant and transgenic mosaic animals, *gdf6Y* most likely determines the male
95 sex by inhibiting the female gonadal development, for example by suppressing the expression of
96 the oogenesis-initiating germ cell (GC) factor *foxl2l* (Nishimura et al. 2015; Kikuchi et al. 2019;
97 Kikuchi et al. 2020). This is probably facilitated by genes directly regulated in response to Gdf6Y
98 e.g., *id1* and *zfp36l2*, which we identified in a cell culture-based approach.

99

100 **RESULTS**

101 **The disruption of *gdf6Y* leads to full male-to-female sex reversal**

102 Being the only annotated gene at the peak of Y-specific sequence variation in the *N. furzeri* strain
103 with the smallest SD region (SDR; MZM0403) and the gene with the strongest signal of positive
104 selection in the SDR of the hereafter used, genome-sequenced strain GRZ, *gdf6Y* was proposed as
105 the SD gene in *N. furzeri* (Reichwald et al. 2015). To test whether *gdf6Y* is indeed the male sex
106 determinant in *N. furzeri*, we employed Cas9 and two sgRNAs specifically targeting three non-
107 synonymous or one synonymous SNP in the 2nd exon of *gdf6Y* (Fig. 1 A). This approach led to the
108 highly unlikely result of 16 female and no male fish ($P = 1.53 \times 10^{-5}$; Fig. 1 B). Eight out of
109 these sixteen females had XY chromosomes with an average mutation rate of 97 % in *gdf6Y* only,
110 as determined by cloning the heterogeneous PCR products derived from the target locus and
111 sequencing several clones (Supplemental Fig. S1 B, C, D). In contrast, the eight animals with XX
112 chromosomes had no mutations in *gdf6X* that were detectable with either a T7 endonuclease I
113 assay or by sequencing the PCR product (Supplemental Fig. S1 B, E, F), indicating that the
114 inactivation was very efficient and highly specific. The thus generated, phenotypically female
115 animals with XY chromosomes and an impaired *gdf6Y* are hereafter called phenofemales (XY*).
116 The mosaic phenofemales had gonads, which were histologically indistinguishable from female
117 ovaries (Fig. 1 C) and were fertile. Interestingly, either different frameshift mutations or an in-
118 frame 9 bp deletion in the CDS of *gdf6Y*'s prodomain consistently resulted in the same phenotype
119 (Fig. 1 D; Supplemental Tab. S1). Furthermore, the phenofemales had significantly reduced *gdf6Y*
120 transcript levels compared to males and showed no difference from females in the gonadal
121 expression of sex-specific marker genes (Fig. 1 E, F). Taken together, the inactivation of *gdf6Y*

122 led to full male-to-female sex reversal, which confirms *gdf6Y* as the major male sex determinant
123 in *N. furzeri*.

124

125 **YY* embryos show anomalies in eye and body axis development**

126 According to Mendelian ratios, we expected animals with two Y-chromosomes (YY*) among the
127 offspring of phenofemales and males (Fig. 2 A). As their adult progeny consisted only of males
128 (XY), females (XX), and phenofemales (XY*) in equal ratio, we monitored the development of
129 the phenofemales' clutches and observed malformations of the eye and tail within the egg during
130 organogenesis in about one-quarter of the embryos (Fig. 2 A; Supplemental Fig. S2 A). Those
131 embryos died before hatching and were identified as the YY* animals (Supplemental Fig. S2 B).
132 The YY* typical malformations were characterized by a lacking tail fin development and
133 pigmentation as well as an incomplete closure of the optic fissure leading to a coloboma-like
134 phenotype (Fig. 2 A; Supplemental Fig. S2 C). A histological comparison with normally
135 developing animals at 0 dph also revealed a decreased thickness of retinal layers in the YY*
136 embryos' eyes (Supplemental Fig. S2 D).

137 As *GDF6* orthologs are known to be involved in eye, joint, and melanocyte formation in various
138 species (Settle et al. 2003; Asai-Coakwell et al. 2009; den Hollander et al. 2010; Gramann et al.
139 2019), we wondered whether the lack of *gdf6X* in YY* embryos contributes to their malformations.
140 To address this question, we employed Cas9 and two sgRNAs targeting the same positions
141 previously used to disrupt *gdf6Y* but on the X-chromosome (Fig. 2 B). Using the Synthego ICE
142 (Inference of CRISPR Editing) analysis tool (v3), we estimated an average mutation rate of 97 %
143 and 14 % in *gdf6X* and *gdf6Y*, respectively, indicating that the inactivation of *gdf6X* was as efficient

144 but not as specific as in the case of *gdf6Y* (Supplemental Fig. S2 E). Hence, we observed
145 phenotypes in about one-third of the mosaic males and two-thirds of the mosaic females
146 (Supplemental Fig. S2 F). Two out of ten mosaic males had one-sided microphthalmia, a probably
147 clonal phenotype that was not passed on to subsequent generations. Furthermore, six out of nine
148 mosaic females and one male did not straighten their body axes after hatching, which lead to a
149 curled tail that disabled normal swimming. This detrimental phenotype was also found at varying
150 degrees in all analyzed homozygous hatchlings (X*X*) of the isolated *gdf6X* frameshift mutant
151 line (Fig. 2 C, E; Supplemental Tab. S1) and *gdf6X*/*gdf6Y* double mutant offspring (X*Y*) of
152 phenofemales and mosaic *gdf6X* mutant males (Supplemental Fig. S2 G). However, this curled
153 phenotype was fully compensated not only in female (XX*) but also in male (X*Y) heterozygous
154 animals (Fig. 2 D), indicating that *gdf6Y*, aside from its SD function, can functionally compensate
155 *gdf6X* inactivation. Thus, the lack of *gdf6X* does not contribute to the phenotype of the YY*
156 embryos, which have one functional *gdf6Y* copy.

157 As the phenofemales were generated in the genome-sequenced strain GRZ, the detrimental
158 phenotype of the YY* embryos could be caused by defects in or a dysregulation of the 339 genes
159 annotated in the strain's 26.1 Mb large SDR (sgr05: 15,031,832–41,162,746; Reichwald et al.
160 (2015)). To investigate whether genes in the SDR have a sex chromosome-specific and copy
161 number-dependent regulation, previously published transcriptome data from male and female
162 whole embryos at 10 dpf were consulted (Reichwald et al. 2015). The expression of the most
163 significantly up- and downregulated genes between males and females within the SDR was
164 analyzed in phenofemales and YY* embryos at 11 dpf (Supplemental Fig. S2 H). We found that
165 the most significantly upregulated gene in females, *rnf19a*, indeed showed an X chromosome-
166 dependent expression, while the most downregulated gene, *pctp*, showed an increased expression

167 only in the presence of a Y chromosome. Thus, the sequence changes accumulating on the Y
168 chromosome can lead to both a locally enhanced and reduced gene expression, potentially
169 interfering with the development of YY* embryos.

170 Given that *gdf6X* and *gdf6Y*, apart from SD, seem to be functionally equivalent, we assessed the
171 signaling activities of the respective proteins using a heterologous cellular reporter system (Herpin
172 et al. 2021). To this end, medaka cells harboring different Gal4-Smad fusion proteins (Smad1, 2,
173 3, 5, and 9) and a responsive luciferase reporter were transfected with expression plasmids for
174 *gdf6X* and *gdf6Y* as well as two *gdf6Y* mutants as controls. Compared to the two *gdf6Y* mutant
175 variants both *gdf6X* and *gdf6Y* showed similar signaling properties by significantly inducing the
176 activation of Smad2, 3, and 9 (Fig. 2 F). Notably, Smad2 activation by Gdf6Y led to significantly
177 higher luciferase activity than activation by Gdf6X. Therefore, Gdf6Y's SD function did probably
178 not evolve by an entire switch of the involved TGF-β signaling partners but could have been
179 promoted by enhanced Gdf6Y signaling capabilities.

180

181 **A subset of the testicular somatic supporting cells expresses *gdf6Y***

182 As *gdf6Y* covers the functions of *gdf6X* and additionally determines the male sex in *N. furzeri*, we
183 were interested in how it governs sexual development. It was previously shown that *gdf6Y* is
184 expressed in adult testes while *gdf6X* is not expressed in adult gonads (Reichwald et al. (2015);
185 Supplemental Fig. S3 A). To address the cellular localization of *gdf6Y*'s testicular expression, we
186 used RNAscope as a very sensitive and specific *in situ* hybridization technique. Applying a *gdf6Y*-
187 specific probe together with probes for the GC marker *ddx4* and one of the somatic cell markers
188 *amh*, *dmrt1*, or *wt1a* (Kobayashi et al. 2004; Kluver et al. 2007; Kluver et al. 2009), we found that

189 *gdf6Y* is co-expressed with all three somatic cell markers in proximity to the spermatogonia of the
190 adult testes (Fig. 3 A; Supplemental Fig. S3 B, C). Next, we analyzed the gonadal expression of
191 *gdf6Y* at 0 dph. Marking the GCs with *ddx4* and the somatic cells with *amh*, *dmrt1*, or *wt1a*, we
192 observed that *gdf6Y* is expressed in a subset of the latter in the still largely undifferentiated male
193 gonads (Fig. 3 B; Supplemental Fig. S3 D, E). In contrast to this, the female gonads at 0 dph, where
194 *gdf6Y* is not expressed, are larger and more differentiated due to a greater cell number and already
195 developing oocytes, respectively (Supplemental Fig. S3 F). Taken together, *gdf6Y* expression in
196 both the developing as well as the adult testes was observed in somatic supporting cells.

197 In contrast to *gdf6Y* and *gdf6X*, their upstream neighbor *sybu* is expressed in oocytes of the
198 developing and adult ovaries (Supplemental Fig. S3 G, H), where its mRNA localizes to the vegetal
199 pole contributing to dorsal determination of the embryo (Nojima et al. 2010; Colozza and De
200 Robertis 2014; Oh and Houston 2017). To analyze DNA methylation as a potential cause of the
201 differential expression of *gdf6X* and *gdf6Y* as well as *sybu* in adult gonads, bisulfite sequencing of
202 the region between *gdf6X/Y* and *sybu* was performed on gonadal tissues from males, females, and
203 phenofemales (Supplemental Fig. S4 A, B). While the identified DNA methylation patterns were
204 highly symmetrical on both DNA strands, we found that neither the promoter of *gdf6X* nor *gdf6Y*
205 was methylated in any of the analyzed sexes (Supplemental Fig. S4 A, B). Conversely, the *sybu*
206 promoter was hypomethylated on the X but hypermethylated on the Y chromosome, which
207 translated to a strictly X-chromosomal expression in testes (Supplemental Fig. S4 B, C). In
208 phenofemales however, the methylation of the *sybu* promoter on the Y chromosome decreased
209 compared to males (Supplemental Fig. S4 B). Therefore, *sybu* transcripts from the Y chromosome
210 were also sequence verified in phenofemale ovaries (Supplemental Fig. S4 C). An explanation for
211 the altered Y-chromosomal methylation in phenofemales could be demethylation in the maternal

212 germline and the adoption of the methylation pattern from the paternal X chromosome, as passive
213 maternal demethylation and a take-over of the paternal methylome was shown in zebrafish (Jiang
214 et al. (2013); reviewed in Ortega-Recalde and Hore (2019)). This implies that the silenced genes
215 of the Y chromosome are reactivated in phenofemales. The intergenic region between *sybu* and
216 *gdf6X* or *gdf6Y*, which contains two Y-specific transposable elements (TEs; Supplemental Fig. S4
217 A) was strongly methylated at all analyzed positions, suggesting a transcriptional insulation of the
218 two promoters. Notably, we found that *sybu* transcript variants are sex-specific in *N. furzeri* gonads
219 with the shortest one (NCBI Reference Sequence: XM_015949384.2), which has an alternative
220 transcription start site, being ovary-specific (Supplemental Fig. S4 C). In conclusion, upstream
221 methylation does not seem to control the differential testicular expression of *gdf6X* and *gdf6Y*.

222

223 **Gdf6Y suppresses the onset of female development prior to hatching**

224 To understand the ongoing molecular processes in the developing gonads, we analyzed previously
225 published transcriptome data (Reichwald et al. 2015). Differentially expressed genes (DEGs)
226 between males and females were identified at three different developmental stages, namely the
227 pharyngula stage during organogenesis at 10 dpf, the hatching stage (0 dph), and the larval stage
228 at 3 dph. In the whole embryo at 10 dpf, 3 transcripts were already noticeably upregulated in males
229 and continued to do so in all stages (Supplemental Fig. S5 A). In phenofemales, those transcripts
230 were expressed like in males and, therefore, are not involved in *gdf6Y*-driven sex determination in
231 *N. furzeri* (Supplemental Fig. S5 B). In male trunk parts, 147 and 133 genes were upregulated at 0
232 and 3 dph, respectively (Supplemental Fig. S5 A). In contrast, the number of upregulated genes in
233 female trunks was higher and increased from 322 to 1079 from 0 to 3 dph, respectively
234 (Supplemental Fig. S5 A). From the identified DEGs at 0 dph 35.4 % of the female-specific and

235 10.9 % of the male-specific transcripts were recalled at 3 dph (Supplemental Fig. S5 C). We
236 performed an overrepresentation analysis (ORA) to obtain enriched KEGG (Kyoto Encyclopedia
237 of Genes and Genomes) pathways for the upregulated genes in males and females at 0 and 3 dph.
238 In males, the most enriched pathway was steroid biosynthesis at 0 dph (Supplemental Fig. S5 D).
239 Expectedly, no significantly enriched pathways were identified at 3 dph given the little overlap of
240 male-specific transcripts between the two time points (Supplemental Fig. S5 C). In females,
241 pathways related to cell cycle, DNA repair, meiosis, and oocyte maturation were enriched at 0 and
242 3 dph despite the incomplete overlap of DEGs between both time points (Supplemental Fig. S5 C,
243 E, F). This result validates our observation of an already occurring oogenesis in female gonads at
244 0 dph from the *in situ* hybridization experiments (Fig. 3 B; Supplemental Fig. S3 F). Therefore,
245 the animals' sex is already determined at 0 dph, while the maintenance of *gdf6Y* expression until
246 adulthood suggests that it might be reversible.

247 In medaka, *foxl2l* is a GC-intrinsic factor that promotes oogenesis by inducing *rec8a* and
248 suppressing spermatogenesis (Nishimura et al. 2015; Kikuchi et al. 2019; Kikuchi et al. 2020). At
249 0 and 3 dph, the *N. furzeri* ortholog of *foxl2l* and its putative target gene *rec8* were among the
250 significant DEGs (Supplemental Fig. S5 A). In contrast to the female somatic cell marker *foxl2*
251 and like in medaka, *foxl2l* is upregulated in females at 0 and 3 dph but not in adult gonads (Fig. 1
252 F; Fig. 4 A; Supplemental Fig. S6 A). Analyzing trunk parts at 0 dph and adult gonads, we showed
253 that *foxl2l* is regulated the same way in phenofemales as it is in females, which places the gene
254 downstream of *gdf6Y* (Fig. 4 B). Furthermore, RNAscope analyses confirmed a *foxl2l* expression
255 in ovarian GCs at 0 dph by co-localization with *ddx4* (Fig. 4 C). We also observed *foxl2l* expression
256 in testicular GCs in proximity to *gdf6Y* expressing somatic cells in one out of six analyzed male
257 individuals at 0 dph (Fig. 4 D). This observation suggests that Gdf6Y could affect the expression

258 in GCs, probably leading to *foxl2l* suppression. Searching for *foxl2l* expression foci in adult
259 gonads, we found a single undifferentiated *foxl2l* positive GC in an ovary and none in testes
260 (Supplemental Fig. S6 B). To verify that *foxl2l* influences SD in *N. furzeri* like in medaka, we
261 employed Cas9 and two sgRNAs simultaneously targeting the single exon of *foxl2l* in males,
262 females, and phenofemales. This approach led to various indels disrupting the gene with an
263 efficiency of 63 % on average (Supplemental Fig. S6 C, D). Next, we analyzed the expression of
264 sex-linked genes in the trunk parts of the mosaic *foxl2l* mutants at 0 dph. While neither *gdf6X* nor
265 *gdf6Y* expression was changed in the mutants of all sexes, we observed a significant decrease of
266 marker genes for cell division (*tacc3*) and oocyte development (*zp3/4*, *sybu*) to nearly male levels
267 in the mutant females and phenofemales (Fig. 4 E; Supplemental Fig. S6 E, F). The aromatase
268 gene *cyp19a1a* and the meiosis marker *rec8*, a putative target of *foxl2l*, decreased only in some
269 but not all mutant females and phenofemales (Supplemental Fig. S6 F). Taking the mosaic nature
270 of the mutants into account, this data supports that *foxl2l* promotes oogenesis in *N. furzeri* and acts
271 downstream of *gdf6Y*.

272 To investigate, if the presence of *gdf6Y* is sufficient to suppress oogenesis in *N. furzeri*
273 development, we used Tol2 transgenesis to drive *gdf6Y* expression under the control of a
274 ubiquitous *actb2* promoter from *D. rerio* (Supplemental Fig. S6 G; Hartmann and Englert (2012)).
275 Analyzing the trunk parts of transgene-positive mosaic animals at 0 dph, we found that the
276 expression of the female-specific genes *rec8*, *zp3/4*, and *sybu* was significantly decreased in
277 transgenic XX animals compared to non-transgenic females (Supplemental Fig. S6 H). The
278 aromatase gene *cyp19a1a* decreased only in some but not all transgenic females (Supplemental
279 Fig. S6 H). Furthermore, the *gdf6Y* expression of both XX and XY transgenic animals was much
280 higher than in the non-transgenic males due to the ubiquitous expression (Supplemental Fig. S6 I).

281 Hatching the mosaic *gdf6Y* transgenic animals, we observed that the hatchlings failed to straighten
282 their body axes and were not able to swim normally (Supplemental Fig. S6 J). This detrimental
283 phenotype was reminiscent of the homozygous loss of function (Fig. 2 E; Supplemental Fig. S2
284 H), suggesting that tight spatiotemporal regulation of the *gdf6* alleles is necessary for proper
285 development in *N. furzeri*.

286

287 **Gdf6Y-responsive genes are differentially expressed between female and male *N. furzeri***

288 To identify Gdf6Y target genes, we transfected cell lines with a *gdf6Y* expression plasmid or one
289 out of two control plasmids and analyzed their transcriptomes after 24 h. As a model for the
290 somatic cells, which express *gdf6Y* in the killifish's testes, we used murine Sertoli-like TM4 cells
291 (Mather 1980). The transcriptome of TM4 cells transfected with the *gdf6Y* expression plasmid was
292 compared with the transcriptome of TM4 cells either expressing the *gdf6Y* mutant variant $gdf6Y^{del9}$
293 or carrying an empty vector (EV). Overlaps of the DEGs from both comparisons resulted in 20 up-
294 and 22 downregulated genes in the presence of *gdf6Y* (Fig. 5 A; Supplemental Fig. S7 A). An
295 overrepresentation analysis revealed TGF-β signaling as the most enriched pathway among those
296 42 DEGs (Fig. 5 B). Out of the 7 genes assigned to this pathway, only *Tgfbr2* was downregulated,
297 while *Id1*, *Id2*, *Id3*, *Smad6*, *Smad7*, and *Smad9* were upregulated (Fig. 5 A). With *Id1*, *Id2*, and
298 *Id3* being known downstream effectors of BMPs (Hollnagel et al. 1999; Yang et al. 2013), this
299 suggests that these genes are regulated as an immediate response to Gdf6Y-signaling. To verify
300 the Gdf6Y-responsive genes that we had identified, we performed the same experiment in human
301 HeLa cells (Fig. 5 C; Supplemental Fig. S7 B). Here, 6 commonly upregulated orthologous genes
302 were identified, namely *Lxn*, *Id1*, *Id2*, *Id3*, and the inhibitory (I-) Smad-genes *Smad6* and *Smad7*,
303 of which the latter 5 were previously assigned to the TGF-β signaling pathway (Fig. 5 A). The

304 single commonly downregulated orthologous gene was *Zfp36l2*, which encodes a zinc finger
305 protein that binds to AU-rich elements (AREs) in the 3' untranslated regions (UTRs) of mRNAs
306 promoting their degradation (Hudson et al. 2004). Expression analysis in accordingly treated
307 human HEK293 cells confirmed the regulation of all these orthologous genes but *ID2* in the
308 presence of *gdf6Y*, verifying them as general Gdf6Y-response genes (Supplemental Fig. S7 C).
309 Next, we assessed their potential role in *N. furzeri* sex determination by examining the sex-specific
310 expression of their orthologs in different tissues and developmental stages utilizing the previously
311 published transcriptome data from Reichwald et al. (2015). While no reads had been mapped for
312 the orthologs of *Id2* and *Lxn*, we found that *id1* was upregulated in male embryos at 10 dpf and
313 *zfp36l2* was downregulated in testes of 3-month-old animals, corresponding to the *gdf6Y*-
314 dependent regulation observed in the cell culture-based approach (Fig 5 D; Supplemental Fig. S7
315 D). Furthermore, the male-specific downregulation of *zfp36l2* in the gonad was reversed in
316 phenofemales carrying either the *gdf6Y* mutant variant $gdf6Y^{del9}$ (Fig 5 E) or the frameshift
317 mutation $gdf6Y^{del113}$ (Supplemental Fig. S7 E). These data suggest that the identified Gdf6Y-
318 response genes, especially *id1*, and *zfp36l2*, are involved in *N. furzeri* sex determination.

319

320 **DISCUSSION**

321 Employing CRISPR/Cas9-mediated gene inactivation and overexpression obtaining full XY male-
322 to-female and partial XX female-to-male sex reversals, respectively, we demonstrate that *gdf6Y* is
323 necessary and sufficient for sex determination in *N. furzeri*. Among the identified *gdf6Y* mutations
324 causing a male-to-female sex reversal, we found a 9 bp in-frame deletion within the prodomain
325 ($gdf6Y^{del9}$), which leads to the loss of amino acids 199 to 201. These amino acids are highly
326 conserved among vertebrate *gdf6* orthologs and a heterozygous point mutation altering one of them

327 leads to microphthalmia in humans (Asai-Coakwell et al. 2009). While not directly affecting the
328 mature ligand, these residues might be important for prodomain folding and the release of the
329 ligand from the proprotein complex, which is required for signaling. All other isolated *gdf6Y*
330 mutants carried frameshift mutations leading to premature termination in the latter half of the
331 prodomain. Similar frameshift mutations in *gdf6b* also led to male-to-female sex reversal in the
332 Pachón cavefish *Astyanax mexicanus* (Imarazene et al. 2021), which harbors two *gdf6* paralogs,
333 *gdf6a*, and *gdf6b*. While the SD gene in *A. mexicanus* arose from an additional *gdf6b* duplicate on
334 a supernumerary B chromosome, *gdf6Y* and conversely *gdf6X* emerged through allelic
335 diversification from an ancient *gdf6a* as no *gdf6b* ortholog is present in the available *N. furzeri*
336 genome sequences (Reichwald et al. 2015; Valenzano et al. 2015).

337 While *gdf6Y* compensates for the loss of *gdf6X*, it also adopted the SD function in *N. furzeri* and
338 possibly its sister species *N. kadleci,* which shares *N. furzeri*'s sex chromosomes (Stundlova et al.
339 2022). Three possible scenarios of how *gdf6Y*'s SD function evolved are functional alterations to
340 the amino acid sequence, changes in the spatiotemporal gene expression, or a combination of both.
341 The positive selection of *gdf6Y* in the SDR and the conservation of non-synonymous SNPs among
342 strains support the theory of an allelic neofunctionalization (Reichwald et al. 2015). Structural
343 modeling suggested that the four most C-terminal amino acid substitutions in Gdf6Y affect
344 dimerization or ligand-receptor binding (Reichwald et al. 2015). We found that Smad2 activation
345 by Gdf6Y was significantly increased compared to Gdf6X. Interestingly, a substitution of a highly
346 conserved tyrosine for asparagine in human GDF6 was reported to decrease its sensitivity for the
347 inhibitor Noggin (Wang et al. 2016). In *N. furzeri*, this residue is surrounded by the last two
348 substitutions between Gdf6X and Gdf6Y, suggesting decreased inhibitor sensitivity as an
349 explanation for Gdf6Y's enhanced signaling capability. On the other hand, we confirmed the

350 expression of *gdf6Y* but not *gdf6X* in adult *N. furzeri* testes, implying a differential regulation of
351 the genes. We investigated DNA methylation as a potential cause of the differential expression of
352 *N. furzeri*'s *gdf6* alleles in testes. While X-chromosomal hypermethylation of the SDR is crucial
353 for sex determination in the channel catfish *Ictalurus punctatus* (Wang et al. 2022), the promoters
354 of both *gdf6Y* and *gdf6X* are hypomethylated in gonads. The hypermethylation of the *sybu*
355 promoter on the Y chromosome on the other hand indicates transcriptional silencing of *N. furzeri*'s
356 Y-chromosome outside of the SD locus, suggesting an explanation for the lack of *rnf19a*
357 expression in YY* embryos. The intergenic region between *gdf6X/gdf6Y* and *sybu* was highly
358 methylated on both sex chromosomes. Therefore, the two Y-exclusive TEs in this region might
359 not harbor *gdf6Y*-specific upstream enhancers, as enhancer activity would require a low or at most
360 intermediate DNA methylation (Sharifi-Zarchi et al. 2017). In other fish species, TEs contribute
361 sex-specific positive and negative regulatory elements that are crucial to SD gene function (Herpin
362 et al. 2010; Herpin et al. 2021). Given that TEs accumulate on fish sex chromosomes during their
363 early evolution (Chalopin et al. 2015) and contribute to the suppression of meiotic recombination
364 (reviewed in Kent et al. (2017)), they could also cause an aberrant expression of non-SD genes in
365 the SDR e.g., the Y-dependent expression of *pctp* in *N. furzeri* embryos. However, the Y-
366 chromosomal effects on the expression of *rnf19a* and *pctp* might be GRZ-specific, as SDRs of
367 other strains differ in size with the smallest containing only one gene, which is *gdf6Y* (Reichwald
368 et al. 2015). Even allelic SNPs in *sybu* are not sex-linked in all strains (Reichwald et al. 2015).
369 Therefore, the severe phenotype of YY* embryos would likely not occur in strains with smaller
370 SDRs. Conversely, regulatory elements, causing the testis-specific expression of *gdf6Y*, should be
371 located within the minimal SDR, which also contains a gene desert downstream of the gene itself.
372 This well-conserved gene desert harbors most cis-regulatory elements controlling *GDF6*

373 expression in other vertebrates (Mortlock et al. 2003; Portnoy et al. 2005; Pregizer and Mortlock
374 2009; Reed and Mortlock 2010; Indjeian et al. 2016; Bademci et al. 2020; Mortlock et al. 2022).
375 Therefore, changes in or the acquisition of new Y-chromosomal enhancers downstream of *gdf6Y*
376 are potential causes of its sex-specific expression. Whether protein or expression changes evolved
377 first and which event constituted *gdf6Y* as the SD gene are open questions, but both probably
378 played a role in its fixation.

379 Vertebrate sex determination is believed to be initiated by the sexual fate decision of the somatic
380 cells of the bipotential gonadal primordium, which in turn control female or male gametogenesis.
381 In a trade-off between male and female regulatory networks involving *Dmrt1* on the male and
382 *Foxl2* on the female side, the equilibrium tips to one side by varying SD factors in different species
383 (Herpin and Schartl 2015). In *N. furzeri*, *gdf6Y* is the male SD gene and is expressed in testicular
384 somatic cells. In a cell culture-based approach murine Sertoli-like cells were used to identify
385 Gdf6Y targets. In a complementary approach, Wang et al. (2022) analyzed gene expression in
386 response to BMP signaling inhibition in human testis cells from 7-week-old fetuses, which is one
387 to two weeks past the arrival of the migrating GCs in the genital ridge and, thereby, shortly after
388 sex determination. As in our data, *ID1/2/3*, *SMAD6/7/9*, and *UNC5B* were upregulated in a BMP-
389 dependent manner. However, only *UNC5B* was Sertoli cell-specific, while the other genes were
390 regulated in all somatic and GC populations, showing the omnipresence of BMP signaling in the
391 developing testis. This is consistent with our observation that *Id1/2/3* and *Smad6/7* are expressed
392 in response to Gdf6Y, independent of cell type. *Arapaima gigas* provided evidence for the
393 involvement of *ID* genes in sex determination in teleost species with a Y-chromosomal *id2b*
394 duplicate being its SD gene (Adolfi et al. 2021). In *N. furzeri*, *id3* is positively selected like *gdf6Y*,
395 suggesting a potential co-evolution (Reichwald et al. 2015). However, we found *id1* upregulated

396 in male *N. furzeri* embryos at 10 dpf, indicating a role of Gdf6Y in paracrine signaling to the GCs
397 during sex determination or sexual development. In mammals, *N. furzeri*, medaka, and zebrafish,
398 female GCs enter meiosis during early gonadal development, while male GCs do not until puberty.
399 Regarding the determination of the GCs' sexual fate, *foxl2l* was identified as a GC-intrinsic
400 feminizing factor in medaka, where the gene's inactivation leads to a GC-specific female-to-male
401 sex reversal and the development of sperm in ovaries that failed to initiate oogenesis at the regular
402 developmental time point (Nishimura et al. 2015). While *foxl2l* inactivation in tilapia
403 (*Oreochromis niloticus*) leads to a similar phenotype, it leads to a full female-to-male sex reversal
404 in zebrafish (Dai et al. 2021; Liu et al. 2022). In *N. furzeri*, *foxl2l* is also involved in female GC
405 sex determination, as shown by the masculinized expression of marker genes in mosaic *foxl2l*
406 inactivated females and phenofemales at 0 dph. In medaka, male and female GCs initially express
407 *foxl2l* at the onset of sexual differentiation of the gonads. While its expression is lost in male GCs,
408 the mitotically active subpopulation of female GCs expresses *foxl2l* until entering meiosis
409 throughout life (Nishimura et al. 2015; Nishimura and Tanaka 2016; Tanaka 2016). The role of
410 *foxl2l*-expressing cells as pre-meiotic oocyte progenitors was confirmed in the zebrafish ovary
411 (Liu et al. 2022). In *N. furzeri*, we also detected *foxl2l* expression in female GCs but not oocytes
412 during ovarian development at 0 dph and in adulthood. In contrast, we rarely found *foxl2l*
413 expressing GCs in developing testes at 0 dph and never in adult testes, supporting that its female
414 GC SD function is conserved in *N. furzeri*. As the gonadal somatic cells direct GC fate during sex
415 determination, Gdf6Y might be the somatic cell signal that initiates male GC fate and suppresses
416 *foxl2l* expression. Therefore, *foxl2l* should be directly or indirectly downregulated by Gdf6Y-
417 responsive genes like *id1*, which shows a male-specific expression at 10 dpf. In human fetal
418 gonads, expression of TGF-β signaling pathway genes including *ID1/2/3* is enriched in both female

419 and male GCs (Li et al. 2017). This observed TGF-β signaling was attributed to AMH from Sertoli
420 cells in males and BMP2 from granulosa cells in females (Li et al. 2017). We detected *amh*
421 expression in both types of somatic supporting cells in male and female *N. furzeri*. While AMH
422 signals via the phosphorylation of the typical BMP-activated Smads 1, 5, and 9 (di Clemente et al.
423 2003; Orvis et al. 2008), Gdf6Y led to the phosphorylation of Smad9, Smad3, and Smad2 in an
424 enhanced manner compared to Gdf6X. Interestingly, Smad2 is important in male GC sex
425 determination in mice, where it is probably activated by the TGF-β family members activin and
426 nodal (Wu et al. 2015). In *N. furzeri*, Gdf6Y could replace or interfere with this signaling. We also
427 identified one downregulated gene in response to Gdf6Y: *zfp36l2*. It encodes an mRNA decay
428 activator and is expressed in developing oocytes, where it is involved in meiotic cell cycle
429 progression and oocyte maturation (Belloc and Mendez 2008; Ball et al. 2014; Ball et al. 2017;
430 Sha et al. 2018), explaining its expression in *N. furzeri* female and phenofemale ovaries compared
431 to testes. Zfp36l2 also controls epigenetic changes in the oocyte by regulating transcripts of histone
432 and DNA demethylases (Chousal et al. 2018). While this takes place after sex determination,
433 *zfp36l2* is female GC-specific and could influence gene expression on the transcriptional or
434 indirectly the epigenetic level during GC sex determination. Overall, our data suggest that *gdf6Y*
435 determines the male sex by suppressing female ovarian development. A similar mechanism was
436 shown for the transcription factor SdY, which directly interacts with Foxl2 to suppress female
437 differentiation in the gonadal somatic cells of *O. mykiss* (Bertho et al. 2018). However, while
438 Gdf6Y could signal to both germ and somatic cells, our data suggests that it suppresses female
439 differentiation of GCs instead of somatic cell.

440

441 **DATA AVAILABILITY**

442 The RNA and bisulfite sequencing data discussed in this publication and applied in-house scripts
443 are available on request.

444

445 **AUTHOR CONTRIBUTIONS**

446 Conceptualization, A.R., C.E.; methodology, A.R.; software, R.S., P.K.; Formal Analysis, A.R.,
447 R.G., P.K., A.P.; investigation, A.R., H.M., M.T., M.K., R.G., C.A., N.H., A.H.; data curation,
448 A.R., H.M., M.T., M.K., R.G., C.A., P.K., M.G., A.P.; writing – original draft, A.R.; writing –
449 review & editing, A.R., C.E.; visualization, A.R.; supervision, C.E.; funding acquisition, C.E.

450

451 **ACKNOWLEDGEMENTS**

452 We thank Christina Ebert, Sabine Matz, Sabine Landmann-Weinsheimer, Silke Foerste, Peter
453 Singer, Joseph Kölbel, and Gabriele Günther for their excellent technical support, and Hanna
454 Reuter for her bioinformatical expertise. We are very grateful to members of the Core Facilities
455 Next Generation Sequencing (Ivonne Goerlich, Cornelia Luge, and Martin Bens), Life Science
456 Computing, and Imaging for their contributions. We also thank the members of FLI's fish facility,
457 most notably Simone Dunkel, Martin Neumann, Johannes Wilfert, Marcus Schmidt, Uta
458 Naumann, and Beate Hoppe. This project was supported by a grant (EN 280/15–1) from the
459 Deutsche Forschungsgemeinschaft to CE. The FLI is a member of the Leibniz Association and is
460 financially supported by the Federal Government of Germany and the State of Thuringia.

461

462 **COMPETING INTERESTS**

463 The authors declare no competing interests.

464

465 **MATERIAL AND METHODS**

466 **Experimental Models**

467 **Fish experiments**

468 All animals were maintained in the fish facility of the Leibniz Institute on Aging – Fritz Lipmann
469 Institute Jena according to the German Animal Welfare Law. All experiments were covered by
470 animal experiment licenses 03-005/12, 03-044/16, and FLI-18-020 approved by the Thuringian
471 authorities (Thüringer Landesamt für Verbraucherschutz).

472 All experiments were performed in the *N. furzeri* wild-type strain GRZ (Jubb 1971) or genetically
473 modified lines in this strain background (Supplemental Tab. S1) except for the *in situ* hybridization
474 in Supplemental Fig. S3 G, where MZM0403 was used instead (Terzibasi et al. 2008). Fish were
475 single-housed at 26 °C in a light:dark cycle of 12 h each. Adult fish were once daily fed *ad libitum*
476 with red mosquito larvae. Juveniles up to 5 weeks post-hatching were fed with artemia twice daily.
477 To obtain fertilized GRZ oocytes for injections, breeding groups of five (one male, four females)
478 to ten fish (two males, eight females) were set up in 20 to 40 l tanks, respectively. To obtain oocytes
479 from phenofemales, breeding groups of one male and up to four phenofemales were set up in 8.5
480 l tanks. Sandboxes for egg deposition were removed for two days and placed back into the tank 2
481 h before injection. Eggs were collected with a sieve and used for microinjections. For line
482 maintenance, eggs were collected weekly, put on coconut coir plates, and incubated at 29 °C to

483 develop until 0 dph. For egg storage up to 1 year, eggs were incubated at 25°C to enter diapause
484 and moved to 29 °C for 1 to 2 weeks before hatching.

485 Dechorionation of embryos and animals at 0 dph was performed as described previously (Richter
486 et al. 2022). Phenotypes of embryos and larvae up to 2 dph were documented using reflective or
487 transmission light with the Zeiss SteREO Discovery.V8 equipped with a Zeiss AxioCam MRc and
488 a Volpi dual gooseneck pole mount light or the Zeiss Axio Zoom.V16 equipped with a Zeiss
489 AxioCam HRc and an HXP 200 C light source, respectively. Phenotypes of adult animals were
490 documented with a Canon IXUS 160.

491

492 **Cell culture**

493 TM4, HeLa, and HEK293 cells were cultivated in Dulbecco's Modified Eagle Medium (DMEM;
494 TM4, HeLa: Gibco™ #41966 – high glucose, pyruvate; HEK293: Gibco™ #31966 – high glucose,
495 GlutaMAX™ Supplement, pyruvate) with 10 % FBS at 37 °C and 5 % CO_2. For transfections, 0.5
496 x 10^6 HeLa and TM4 cells or 4 x 10^5 HEK293 cells per well were seeded into 6- or 12-Well plates,
497 respectively. 24 h later, the cells were transfected with 2.5 µg or 1 µg of plasmid DNA (pcDgdf6Y,
498 pcDgdf6Ydel9, or pcDNA3.1-HA) per well of a 6- or 12-Well plate, respectively, using
499 Lipofectamine 3000 (Thermo Fisher Scientific) and incubated for 24 h at 37 °C and 5 % CO_2
500 before RNA isolation.

501 Medaka fibroblast cells were cultured at 28°C and 5% CO2 in DMEM supplemented with high
502 glucose (4.5 g/L), 4 mM glutamine, and 15% FBS as previously described (Thoma et al. 2011).
503 For transfection, cells were grown to 80% confluency in six-well plates and subsequently

504 transfected using either Lipofectamine (Thermo Fisher Scientific) or FuGENE (Roche) reagents
505 as described by the manufacturers.

506

507 **Method Details**

508 **Tol2 transgenesis and CRISPR/Cas9 mutant generation**

509 The plasmid pDTactb2:gdf6Y, which contains the *D. rerio actb2*-promoter driven *gdf6Y*
510 expression cassette, was generated by combining the Tol2kit (Kwan et al. 2007) vectors #395
511 (pDestTol2CG2) and #299 (p5E-*bactin2*) with pMEgdf6Y and p3Egdf6YpA in a Gateway LR
512 Clonase II (Thermo Fisher Scientific) reaction according to the manufacturer's instructions. To
513 generate plasmids pMEgdf6Y and p3Egdf6YpA, the *gdf6Y* genomic sequence from start- to stop-
514 codon (including the intron) or the 965 bp sequence immediately downstream of *gdf6Y*,
515 respectively, were amplified using Phusion High-Fidelity Polymerase (Thermo Fisher Scientific)
516 according to the manufacturer's instructions. The applied oligonucleotides added the respective
517 *att*-sites to recombine the obtained amplicons into pDONR221 (Thermo Fisher Scientific) or
518 pDONRP2R-P3 (Tol2kit #220) for the generation of pMEgdf6Y or p3Egdf6YpA, respectively,
519 using Gateway BP Clonase II (Thermo Fisher Scientific) according to the manufacturer's
520 instructions. *Tol2*- and *EGFP*-mRNA were *in vitro* transcribed as described previously (Hartmann
521 and Englert 2012) and quality-controlled by RNA agarose gel electrophoresis. The injection
522 solution contained 20 ng/µl of pDTactb2:gdf6Y, 10 ng/µl of *Tol2*-mRNA, 30 ng/µl of *GFP*-
523 mRNA, and 0.1 % phenol red.

524 To generate mutants with CRISPR/Cas9, sgRNAs were designed based on previously published
525 X and Y chromosomal sequences (*gdf6Y*- and *gdf6X*-inactivation; Reichwald et al. (2015)) or by

526 utilizing CHOPCHOP v3 (*foxl2l*-inactivation; Labun et al. (2019)). Templates for the *in vitro*
527 transcription of sgRNAs were generated either by subcloning annealed oligonucleotides
528 containing the target sequences into pDR274 (Addgene, plasmid #42250) via *BsaI* as described
529 previously (*gdf6Y*-inactivation; Krug et al. (2023)) or by PCR (*gdf6X*- and *foxl2l*-inactivation). For
530 the PCR, complementary oligonucleotides containing the T7 promoter, the 20 bp sgRNA target
531 sequence, and the sgRNA backbone were applied as template-DNA at a concentration of 0.002
532 µM each and amplified using Phusion High-Fidelity Polymerase in 1X HF-Buffer (Thermo Fisher
533 Scientific) with an additional primer pair (T7F and pDRrvs) according to the manufacturer's
534 instructions. The respective oligonucleotides are listed in Supplemental Tab. S2. The
535 approximately 300 bp *DraI* restriction fragments (*gdf6Y*-inactivation) or the 124 bp amplicons
536 (*gdf6X*- and *foxl2l*-inactivation) were purified from an agarose gel or the PCR, respectively, using
537 the NucleoSpin Gel and PCR Clean-up Mini kit (Macherey-Nagel) according to the
538 manufacturer's instructions. Up to 1 µg purified DNA was *in vitro* transcribed overnight at 37°C
539 with the MAXIscript T7 Transcription Kit (Thermo Fisher Scientific). The synthesized sgRNAs
540 were precipitated from the reaction using Ammonium acetate Stop Solution as described for the
541 mMessage mMachine Kit protocol (Thermo Fisher Scientific). *Cas9*-mRNA was *in vitro*
542 transcribed overnight at 20°C from 400-500 ng *XbaI*-linearized pT3TS-nCas9n (Addgene, plasmid
543 #46757) using the mMessage mMachine T3 Kit (Thermo Fisher Scientific) and purified with the
544 MegaClear Kit (Thermo Fisher Scientific) according to the manufacturer's instructions. All RNAs
545 were quality-controlled by RNA agarose gel electrophoresis. Injection solutions contained 30
546 ng/µl of each sgRNA, 300 ng/µl of *Cas9*-mRNA, 30 ng/µl of *GFP*-mRNA, and 0.1 % phenol red.

547 Microinjections into *N. furzeri* oocytes were performed as described previously by Hartmann and
548 Englert (2012) (*gdf6Y*-inactivation) or Krug et al. (2023) (*gdf6Y*-transgenesis, *gdf6X*- and *foxl2l*-
549 inactivation) applying the injection solutions described above.

550

551 **Molecular sexing and genotyping of animals**

552 Genomic DNA samples were derived from caudal fin biopsies of adult animals or tail tips from
553 embryos and larvae as described previously by Krug et al. (2023) and Richter et al. (2022),
554 respectively. For sexing and genotyping PCRs, DreamTaq DNA Polymerase (Thermo Fisher
555 Scientific) was used according to the manufacturer's instructions with an annealing temperature
556 of 60°C, if not indicated otherwise. Sex chromosomes were determined by either a *gdf6Y*-specific
557 PCR using oligonucleotides Nf_Gdf6m_fw4: 5'-GAGAAAGAGGAGCTGGTCGGG-3' and
558 Nf_Gdf6Y_rv4: 5'-GCGCTGCTGATGATGATGCC-3' (Gonosome PCR in Supplemental Fig.
559 S1 B) or as described previously (see Supplemental Fig. S2 B; Richter et al. (2022)). For the *gdf6Y*-
560 specific PCR, an annealing temperature of 64°C was applied. As the *gdf6Y*-specific PCR flanks
561 the target sites of sgRNA Y1 and Y2, it was also used for genotyping of $gdf6Y^{del6,\ del8}$, and $gdf6Y^{del9}$
562 phenofemales yielding a 205 or 210 bp fragment, respectively, compared to a 219 bp fragment in
563 males. $Gdf6Y^{del113}$ and $gdf6X^{del113}$ mutations were identified by applying oligonucleotides gdf6-
564 gtF2: 5'- GGCCTCTGTGGGAGAATGTG-3' and gdf6-gtR1: 5'- ACCGACCTCCGCGACTTG-
565 3' (Target locus PCR in Supplemental Fig. S1 B, C) indicating the mutant allele by a smaller
566 fragment. Mutations in *foxl2l* were analyzed using oligonucleotides
567 foxl2lt2F: 5'-GAGGTATGGATGCGGATAAGAA-3' and foxl2lt3R: 5'-
568 CTGATGCAGGTAGTAGTCGGTG-3' flanking the sgRNA target sites. *Gdf6Y*-transgenic
569 hatchlings and larvae were identified by the detection of EGFP in the heart by fluorescence

570 microscopy and a transgene-specific 735 bp fragment by PCR applying oligonucleotides
571 gdf6YinsituF1: 5'-CGGAGGGTAACCTGCTGC-3' and M13F: 5'-GTAAAACGACGGCCAG-
572 3' at an annealing temperature of 55°C.

573 To determine mutation rates in *gdf6X/Y* in mosaic XY* animals, the *gdf6X/Y* target locus PCR was
574 either performed as described above or using Phusion High-Fidelity Polymerase (Thermo Fisher
575 Scientific) according to the manufacturer's instructions. The obtained DreamTaq and Phusion
576 amplified fragments were cloned into pCRII-TOPO using the TOPO TA Cloning Kit (Thermo
577 Fisher Scientific) according to the manufacturer's instructions or the pUC57-derivative pGGC
578 (Geissler et al. 2011) via *SmaI* cut-ligation, respectively. Individual clones were Sanger sequenced
579 with M13F in-house by the FLI Core Facility Next Generation Sequencing or externally by
580 Eurofins Genomics TubeSeq Service. *Gdf6X/Y* target locus PCR amplicons from XX animals,
581 injected with the *gdf6Y* sgRNAs Y1 and Y2, were purified from the reaction with NucleoSpin Gel
582 and PCR Clean-up Mini kit (Macherey-Nagel) according to the manufacturer's instructions and
583 subjected to a T7 Endonuclease assay (T7EI) and Sanger sequencing with gdf6-gtF2 by Eurofins
584 Genomics TubeSeq Service. For the T7EI assay, 200 ng of purified PCR product and 1 µl of NEB
585 2 Buffer (New England Biolabs) in 9.5 µl total volume were first denatured for 5 min at 95°C and
586 then rehybridized by cooling the sample at a rate of 2°C/s to 85°C and a rate of 0.1°C to 25°C to
587 obtain potential heteroduplex DNA. To detect potential heteroduplex DNA by cleavage, 0.5 µl of
588 T7EI (New England Biolabs) were applied for 15 min at 37°C and the reaction was analyzed by
589 agarose gel electrophoresis. Sanger sequences from individual clones and PCR products were
590 analyzed with Geneious Prime 2019.2.3.

591 To determine *gdf6X/Y* mutation rates in mosaic animals, injected with the *gdf6X* sgRNAs X1 and
592 X2, the *gdf6Y*-specific and the *gdf6X/Y* target locus PCR were performed on X*Y or X*Y and

593 X*X* individuals, respectively. PCR products were Sanger sequenced with the forward primer of
594 the respective PCR by Eurofins Genomics TubeSeq Service. Sequences of the *gdf6Y*-specific and
595 the *gdf6X/Y* target locus PCR on X*X* animals were analyzed with Synthego Performance
596 Analysis, ICE Analysis. 2019. v3.0. Synthego; [accessed between 03/05/2021 and 03/19/2021] by
597 supplying the sgRNA Y2 or both *gdf6X*-sgRNA sequences, respectively. Sequences of the *gdf6X/Y*
598 target locus PCR on X*Y animals were analyzed with Synthego Performance Analysis, ICE
599 Analysis. 2019. v3.0. Synthego; [accessed between 03/05/2021 and 03/19/2021] by supplying both
600 *gdf6X*-sgRNA sequences and the *gdf6Y*-sequence as a donor sequence to exclude the *gdf6Y* wild-
601 type sequence from analysis of the *gdf6X* mutation rate. The result was evaluated by calculating
602 the mutation rate as the percentage proportion of predicted indel sequences from the sum of indel
603 and wild-type sequences.

604 PCR products from individual *foxl2l*-mosaic mutants were first examined for large indel mutations.
605 Those samples without obvious indels were subjected to a T7EI assay as described above. T7EI-
606 resistant samples were declared as not mutated, while PCR products from cleaved samples were
607 Sanger sequenced with foxl2lt2F by Eurofins Genomics TubeSeq Service. Sequences were
608 analyzed with Synthego Performance Analysis, ICE Analysis. 2019. v3.0. Synthego; [accessed on
609 11/17/2021 and 11/23/2021] by supplying the two *foxl2l*-sgRNA sequences and evaluated as
610 described above.

611

612 **Immunohistochemistry and RNAscope *in situ* hybridization**

613 Dissected gonads and embryos were fixed in 4% paraformaldehyde/PBS overnight at 4°C, washed
614 in phosphate-buffered saline, and paraffin-embedded. 5 μm sections were prepared with the

615 Epredia HM 340 E electronic rotation microtome (Thermo Fisher Scientific) and transferred onto
616 Superfrost Plus Slides (Thermo Fisher Scientific). The prepared sections were stained with
617 Haematoxylin and Eosin (H&E) or used for RNAscope experiments. H&E stainings were imaged
618 and processed with the AxioScan (Zeiss) and ZEN 2.6 (Blue Edition, Zeiss), respectively.

619 For RNAscope experiments, if not stated otherwise, buffers and equipment as well as probes were
620 provided by Advanced Cell Diagnostics (Supplemental Tab. S3). The experiments were performed
621 according to the manufacturer's protocol (Advanced Cell Diagnostics, Document number:
622 323100-USM) except for the following changes: 60°C drying steps at the end of deparaffinization
623 and target retrieval were prolonged from 5 to 30 min. Target retrieval and RNAscope Protease
624 Plus treatment were performed for 15 and 30 min, respectively. After creating a barrier with the
625 ImmEdge hydrophobic barrier pen, specimens were photobleached at 350-425 nm for 5 min with
626 Axio Zoom.V16 or the SteREO Discovery.V8 (Zeiss) to reduce autofluorescence. All washing
627 steps during hybridization and development were carried out three times for 5 min. The
628 counterstaining with DAPI was either performed according to the manufacturer's protocol or by
629 applying and mounting the slides with ProLong Gold antifade reagent with DAPI (Thermo Fisher
630 Scientific). For RNAscope samples, Z-stacks were recorded with a 63 x oil objective at the Axio
631 Imager.Z1 with ApoTome.2 (Zeiss). Images were processed in ZEN 2.6 (Blue Edition, Zeiss) by
632 combining all sections of Z-stack into a maximum-intensity projection.

633

634 **Whole mount *in situ* hybridization**

635 MZM0403 hatchlings at 0 dph were fixed in 4% paraformaldehyde/PBS and processed for whole
636 mount *in situ* hybridization as described previously (Hauptmann and Gerster 1994). The

637 digoxigenin-labeled antisense and sense *sybu* riboprobes were synthesized from a *SacII*- or *SacI*-
638 linearized pGEM-T easy (Promega), which contained an 823 bp cDNA-fragment from *sybu*-
639 mRNA (NCBI Reference Sequence: XM_015949383.2) amplified with oligonucleotides
640 Nf_sybu_fw2: 5'-AGAGGACCATCAGCACCAAC-3' and Nf_sybu_rv6: 5'-
641 CAGGGACTCCAACTTCCT-3', using the plasmids SP6 or T7 promoter, respectively. Prior
642 probe hybridization, samples were bleached in 6 % hydrogen peroxide/PBST for 1 h at room
643 temperature, followed by a 30 min Proteinase K-treatment. After probe detection, hatchlings were
644 again fixed in 4% paraformaldehyde/PBS, taken through a methanol series, equilibrated, and
645 oriented for imaging in a clearing solution (1/3 benzyl benzoate, 2/3 benzyl alcohol). Images were
646 acquired using the Zeiss SteREO Discovery.V8 equipped with a Zeiss AxioCam MRc. Images
647 were processed in ZEN 2.6 (Blue Edition, Zeiss). Sex was determined subsequently by sequencing
648 amplicons generated with oligonucleotides scaffold795_4r: 5'-AAATCCTCTCCTGGCCTACC-
649 3' and scaffold795_3f: 5'-GGCTGGCGAGAGTCTTTCTA-3' at genomic DNA isolated from the
650 individual samples.

651

652 **Bisulfite sequencing**

653 Genomic DNA from testes or ovaries was isolated using the QIAamp DNA Mini Kit (QIAGEN)
654 according to the protocol of the manufacturer. The deamination was performed with the EZ DNA
655 Methylation-Gold Kit (Zymo Research) according to the manufacturer's instructions. After
656 deamination, samples were stored at -20°C. PCRs were performed to amplify the region of interest.
657 The reaction mix was composed of 10 µl MyTaq HS Red Mix (Meridian Bioscience), 2 µl
658 deaminated DNA and the respective oligonucleotides at a concentration of 0.5 µM each in 20 µl
659 total volume, and amplified using the following program: initial denaturation at 95°C for 3 min,

660 30 cycles of denaturation at 95°C for 30 s, annealing at 55°C for 30s and elongation at 72°C for 1
661 min, followed by a final elongation at 72°C for 5 min. Amplicons were quality-controlled by
662 agarose gel electrophoresis and distributed in equal amounts into 8 pools. The amplicons per pool
663 (7 pools of 34 amplicons each, 1 pool of 27 amplicons) were individually tagged by one out of
664 four 3 bp-tags (ATG, GCA, CAT, TGC), which were added to the oligonucleotides used for the
665 amplification. The pools of amplicons were purified using Agencourt AMPure XP magnetic beads
666 (Beckman Coulter) according to the manufacturer's instruction. Amplicons pools were quality
667 checked using the 2100 Bioanalyzer instrument in combination with the DNA 7500 assay (both
668 Agilent Technologies). For each pool, an individually tagged library was prepared from 125 ng of
669 input material using the TruSeq DNA PCR-Free kit (Illumina). Since pools of amplicons do not
670 need to be fragmented, the protocol was started with the "Repair Ends" step. The quantification
671 and quality check of libraries were done as described above. Libraries were pooled and sequenced
672 on the MiSeq system. It ran in 151 cycle/paired-end mode (MiSeq reagent kit v2 - 300 cycles).
673 Sequence information was converted to FASTQ format using bcl2fastq v2.20.0.422.

674

675 **RNA isolation**

676 To isolate RNA from *N. furzeri* gonads and transfected cells, the QIAGEN RNeasy Mini Kit was
677 used. Killifish tissue was lysed in RLT buffer containing β-mercaptoethanol using the QIAGEN
678 TissueLyzer II according to the manufacturer's instructions. Cells were lysed directly in the wells
679 using RLT buffer containing ß-mercaptoethanol. Cell samples were further homogenized using
680 the QIAshredder Kit (QIAGEN). DNase digestion was performed on-column using the RNase-
681 Free DNase Set (QIAGEN) as suggested in the RNeasy Mini Kit protocol. The RNA was eluted
682 in 50 µl DEPC-treated H_2O.

683 Total RNA from embryo and hatchling trunks was extracted by adding TRIzol reagent (Thermo
684 Fisher Scientific) and homogenization with the QIAGEN TissueLyser II. For phase separation, the
685 lysate was incubated for 5 min at room temperature followed by the addition of 0.2 volumes of
686 chloroform relative to the starting amount of TRIzol reagent. The solution was shaken vigorously
687 for at least 15 s, incubated for 3 min at room temperature, and centrifuged for 20 min at 12000 x
688 g at 4°C. The aqueous phase was transferred into a fresh Tube and 1 volume of chloroform was
689 added. Shaking, incubation at room temperature, centrifugation, and transfer of the aqueous phase
690 into a fresh Tube were repeated. Alternatively, the lysate was transferred into Phasemaker tubes
691 (Thermo Fisher Scientific), and the phase separation was performed in a single step according to
692 the manufacturer's instructions. For RNA precipitation, 0.5 µl GlycoBlue Coprecipitant (Thermo
693 Scientific Scientific), 1.1 volumes of isopropanol, and 0.16 volumes of 2 M sodium acetate (pH
694 4.0) were added. After mixing and incubation for 10 min at room temperature, samples were
695 centrifuged for 20 min at 12000 x g and 4°C. The supernatant was removed and 500 µl of 80 %
696 ethanol were added to wash the pellet by vortexing and centrifugation at 7500 x g for 10 min at
697 4°C. The washing step was repeated. The pellet was air-dried for 10-15 min and dissolved in 15
698 to 30 µl of DEPC-treated H_2O. For optimal dissolving of the pellet, the sample was incubated at
699 65°C for 5 min. For RT-qPCR of *foxl2l*, samples were cleaned-up and DNase digested with the
700 QIAGEN RNeasy Mini Kit and the RNase-Free DNase Set (QIAGEN) according to the
701 manufacturer's instructions.

702

703 **Reverse transcription-quantitative PCR (RT-qPCR)**

704 For cDNA Synthesis up to 1 µg of total RNA was used. The reverse transcription was performed
705 using the iScript cDNA Synthesis Kit (Bio-Rad) according to the protocol provided by the
706 manufacturer. RT-qPCR was performed in 384 well plates using the CFX384 Real-Time system
707 (Bio-Rad). Each 10 µl reaction contained 5 µl SYBR GreenER™ qPCR SuperMix Universal
708 (Thermo Fisher Scientific), forward and reverse primer at a concentration of 200 nM each, and up
709 to 5 ng/µl cDNA and was cycled according to the manufacturer's instruction. Annealing
710 temperatures were 60°C or 63°C for *N. furzeri* or human cell assays, respectively. Oligonucleotides
711 and their applications are listed in Supplemental Tab. S4.

712

713 **RNA sequencing**

714 Sequencing of RNA samples was performed using Illumina's next-generation sequencing
715 methodology (Bentley et al. 2008). In detail, DNase digested total RNA from TM4, and HeLa cells
716 was quantified, and quality checked using the Tapestation 4200 instrument in combination with
717 an RNA ScreenTape (both Agilent Technologies). Libraries were prepared from 300 ng total RNA
718 using NEBNext Ultra II Directional RNA Library Preparation Kit in combination with NEBNext
719 Poly(A) mRNA Magnetic Isolation Module and NEBNext Multiplex Oligos for Illumina (Unique
720 Dual Index UMI Adaptors RNA) following the manufacturer's instructions (New England
721 Biolabs). Deviating from the instructions, qPCR was performed for each library prior to final
722 amplification to determine the optimal number of cycles (exponential phase) to avoid over-
723 amplification of the libraries in the final amplification step. The quantification and quality check
724 of libraries was done using the Bioanalyzer 2100 instrument and the D5000 kit (Agilent

725 Technologies). Libraries were pooled and sequenced on a NovaSeq6000. The system ran in 101
726 cycle/single-end/standard loading workflow mode (S1 100 cycle kit v1.5). Sequence information
727 was converted to FASTQ format using bcl2fastq v2.20.0.422.

728

729 **Smad-activation luciferase reporter assay**

730 The luciferase reporter assay to analyze Smad-activation mediated by the different *N. furzeri gdf6*
731 alleles and *gdf6Y* mutant variants was performed as reported previously (Herpin et al. 2021). In
732 short, medaka fibroblast cells in six-well plates were co-transfected with 400 ng of one out of four
733 *gdf6*-expression plasmids (pcDgdf6X, pcDgdf6Y, pcDgdf6Ydel9, or pcDgdf6Yins25), 300 ng of
734 one out of five expression plasmids for fusion proteins consisting of Smad activation and Gal4
735 DNA binding domains (Smad1-AD-GAL4-DBD, Smad2-ADGAL4-DBD, Smad3-AD-GAL4-
736 DBD, Smad5-AD-GAL4-DBD, or Smad8-AD-GAL4-DBD), 300 ng of a firefly luciferase
737 reporter plasmid under the control of a UAS sequence containing minimal promoter (UAS-luc),
738 and 5 ng of a *Gaussia* luciferase expression plasmid for normalization (pCMV-Gluc) per well.
739 After 24 h, cells were washed with 2× phosphate-buffered saline and lysed with 75 µL of passive
740 lysis buffer (Promega), and then subjected to luciferase assay. Firefly luciferase activity was
741 quantified using the Dual-Luciferase Reporter Assay System (Promega) and normalized against
742 *Gaussia* luciferase activity.

743

744 **Quantification and statistical analysis**

745 **RT-qPCR quantification**

746 RT-qPCR results were evaluated using the determined threshold cycles (Ct) and primer
747 efficiencies (E) either by calculating the relative expression (R) of a gene of interest (goi) to a
748 reference gene (ref) with the formula:

749 $$R = \frac{{E_{ref}}^{Ct_{ref}}}{{E_{goi}}^{Ct_{goi}}}$$

750 (Supplemental Fig. S3 A and S4 C) or the fold change (FC) of a goi to one or two reference genes
751 (ref1, ref2) with the formula:

752 $$FC = \frac{{E_{goi}}^{\Delta Ct_{goi}}}{\sqrt[2]{{E_{ref1}}^{\Delta Ct_{ref1}} \cdot {E_{ref2}}^{\Delta Ct_{ref2}}}}$$

753 based on Hellemans et al. (2007) (all other RT-qPCR data).

754

755 **Statistical analyses**

756 Graphical presentation and statistical analyses of RT-qPCR data, retina layer measurements,
757 mutation rates, luciferase assay results and comparisons of individual genes' RPKM from the *N.*
758 *furzeri* RNA-Seq data were realized using GraphPad Prism 9 and the indicated statistical test
759 depending on the scientific question and data structure of the respective assay.

760

761 **Bisulfite sequencing data analyses**

762 For data analyses, two operating systems were used. All Python-based software pool_separator.py,
763 methi.py) was controlled with a SunOS 5.10 system. To analyze their output, R studio was used
764 on a Windows 10 operating system. Merging of the paired-end reads per amplicon pool was done
765 using clc_overlap_reads (CLC-Workbench, QIAGEN). The Python in-house script
766 pool_separator.py was used to separate the amplicons stored in the joined .fastq-files. To supply
767 the script with the necessary information, a .csv-file including the semicolon-separated information
768 (pool; 3 bp-tag; forward primer; reverse primer; sample name) for each line-separated amplicon
769 was generated for each pool. The command to run the Python script is shown below with pool 1
770 as an example:

771 python3 pool_separator.py Ampliconpool1_jointed_test.fq pool1comp.csv

772 The script creates a folder for each amplicon, which contains all .fastq-files of each individual
773 sample. The in-house script methi.py was used to calculate the CpG methylation rates. This script
774 separates X and Y chromosomal reads and detects the chromosome-specific methylation rates for
775 all CpGs of each X and Y separated amplicon. The analysis of each amplicon by the script requires
776 the forward and reverse PCR oligonucleotide sequences, the X- and Y-specific amplicon length,
777 the tag length, the position of all CpGs within the amplicon (comma-separated), a location of a
778 non-CpG cytosine as well as 9 to 10 bp X (p1) and Y (p2) signature sequences (9 – 10 bp). The
779 information is stored in a .txt-file as shown below:

780 forward_primer:
781 reverse_primer:
782 expected_length_p1:
783 expected_length_p2:

784 tag_length:3

785 cpg_pos_p1:

786 cpg_pos_p2:

787 cx_pos_p1:

788 cx_pos_p2:

789 p1:

790 p2:

791

792 The command to run the software methyi.py is shown below:

793 python3 software/methi.py -d fastq_files/ -i sample_name.txt -s

794 The cytosine, which is not in a CpG context, is needed used by methyi.py to estimate the
795 conversion rate of the deamination process and to correct the methylation rate. The program uses
796 the frequency (H) of the non-CpG (CpX, X: cytosine or thymine) to calculate the conversion rate
797 (c) as follows:

798 $$c = \frac{H^{CpX}}{H^{XpX}}$$

799 The median (c_{all}) over all CpG methylation rates of the amplicons from all samples was
800 calculated in R Studio as follows:

801 $$c_{all} = \frac{1}{2}(c_{\frac{n}{2}} + c_{\frac{n}{2}+1})$$

802 $$c_{all} = 0.004112382$$

803 Subsequently, the c_{all} was used to calculate the corrected methylation rate (CpG_{corr}) with a value
804 from 0 to 1 for each CpG:

805 $$CpG_{corr} = \frac{CpG - c_{all}}{1 - c_{all}}$$

806 Alternatively, the methylation rate of a CpG was determined sample-wise with Geneious Prime
807 2019.2.3 by assembling the pool-separated reads to a bisulfite-conversed reference sequence of
808 the respective amplicon and measuring the proportion of cytosines at the given position. The
809 obtained methylation rate was corrected with the formula above.

810 The corrected methylation rates of all analyzed CpGs and samples were visualized using Morpheus
811 (https://software.broadinstitute.org/morpheus).

812

813 **RNA-Seq data analyses**

814 The published RNA-Seq data (ENA: ERR879038 - ERR879056) from male and female *N. furzeri*
815 at different developmental stages (Reichwald et al. 2015) was filtered with sga (parameters:
816 preprocess -q 30 -m 50 --dust; https://github.com/jts/sga). Quality-passed reads were mapped to
817 the *N. furzeri* reference genome using STAR STAR (parameters: --alignIntronMax 100000; Dobin
818 et al. (2013)). DEGs (adjusted p-value < 0.05, Log_2(Fold Change) > 1) between females and males
819 of each individual developmental stage were derived using DESeq2 (Love et al. 2014). DEGs were
820 visualized in volcano plots generated with VolcaNoseR (Goedhart and Luijsterburg (2020);
821 https://huygens.science.uva.nl/VolcaNoseR2/).

822 Analysis of RNA-Seq data of murine TM4 and human HeLa cells. The names of the RNA-Seq
823 reads were extended by their unique molecular identifier (UMI) with UMI-tools' extract command
824 version 1.1.1 (Smith et al. 2017). These modified reads were aligned with STAR 2.7.10a
825 (parameters: --alignIntronMax 100000, --outSJfilterReads Unique, --outSAMmultNmax 1, --

826 outFilterMismatchNoverLmax 0.04) (Dobin et al. 2013) to the *M. musculus* (GRCm39) and *H.*
827 *sapiens* (GRCh38) reference genomes, respectively, with the Ensembl genome annotation release
828 107. PCR duplicates were removed from the alignment results using UMI-tools's dedup command.
829 For each gene, reads that map uniquely to one genomic position were counted with FeatureCounts
830 2.0.3 (multi-mapping or multi-overlapping reads were discarded, stranded mode was set to "–s 2")
831 (Liao et al. 2014). The pairwise comparisons of *gdf6Y*-expressing samples with either *gdf6Y*^{del9}-
832 expressing or empty vector samples were analyzed for differential gene expression. Therefore,
833 DEGs were determined with R 4.1.3 using the package DESeq2 1.34.0 (Love et al. 2014). Only
834 genes that have at least one read count in any of the analyzed samples of a particular comparison
835 were subjected to DESeq2. For each gene, the p-value was calculated using the Wald significance
836 test. The resulting p-values were adjusted for multiple testing with the Benjamini & Hochberg
837 correction (FDR). The log2 fold change (log2FC) values were shrunk with the DESeq2 function
838 lfcShrink(type="apeglm") to control for variance of log2FC estimates for genes with low read
839 counts (Zhu et al. 2019). Genes with an adjusted p-value < 0.05 are considered DEGs. Selected
840 DEGs were visualized by calculating Z-scores (formula: $z = \frac{x-\mu}{\sigma}$, x = individual value, μ =
841 arithmetic mean of all x per gene, σ = standard deviation of all x per gene) from DESeq2-
842 normalized counts and creating a heatmap of those using Morpheus
843 (https://software.broadinstitute.org/morpheus). The overlap analysis of the up- or downregulated
844 DEGs identified in TM4 cells with those identified in the same way in human HeLa cells was
845 based on gene symbols and followed by an ortholog verification in Ensembl release 109.

846 Overrepresentation analyses of KEGG pathways were performed using WebGestalt (WEB-based
847 GEne SeT AnaLysis Toolkit; Liao et al. (2019); https://www.webgestalt.org/). For the *N. furzeri*
848 RNA-Seq data, gene symbols from *D. rerio* orthologs assigned to the genebuild_v1.150922 *N.*

849 *furzeri* annotation (Reichwald et al. 2015; Kelmer Sacramento et al. 2020) were used to search for
850 enriched KEGG pathways in a *D. rerio* organismal background. Therefore, female or male DEGs
851 at the different developmental stages were compared to a reference list of all genes identified in
852 the whole data set. For the TM4 RNA-Seq data, gene symbols of the 42 selected DEGs were
853 compared against the *M. musculus* genome to identify enriched KEGG pathways in that genetic
854 background. Parameters for the enrichment analyses were a minimum number of 5 IDs in a
855 category, a maximum number of 2000 IDs in a category and the Benjamini & Hochberg correction
856 for multiple testing.

857

858 **REFERENCES**

859 Adolfi MC, Du K, Kneitz S, Cabau C, Zahm M, Klopp C, Feron R, Paixao RV, Varela ES, de
860 Almeida FL et al. 2021. A duplicated copy of id2b is an unusual sex-determining candidate
861 gene on the Y chromosome of arapaima (Arapaima gigas). *Sci Rep* **11**: 21544.
862 Api M, Biondi P, Olivotto I, Terzibasi E, Cellerino A, Carnevali O. 2018. Effects of Parental Aging
863 During Embryo Development and Adult Life: The Case of Nothobranchius furzeri.
864 *Zebrafish* **15**: 112-123.
865 Asai-Coakwell M, French CR, Berry KM, Ye M, Koss R, Somerville M, Mueller R, van
866 Heyningen V, Waskiewicz AJ, Lehmann OJ. 2007. GDF6, a novel locus for a spectrum of
867 ocular developmental anomalies. *American journal of human genetics* **80**: 306-315.
868 Asai-Coakwell M, French CR, Ye M, Garcha K, Bigot K, Perera AG, Staehling-Hampton K,
869 Mema SC, Chanda B, Mushegian A et al. 2009. Incomplete penetrance and phenotypic
870 variability characterize Gdf6-attributable oculo-skeletal phenotypes. *Human molecular*
871 *genetics* **18**: 1110-1121.
872 Asai-Coakwell M, March L, Dai XH, Duval M, Lopez I, French CR, Famulski J, De Baere E,
873 Francis PJ, Sundaresan P et al. 2013. Contribution of growth differentiation factor 6-
874 dependent cell survival to early-onset retinal dystrophies. *Human molecular genetics* **22**:
875 1432-1442.
876 Bademci G, Abad C, Cengiz FB, Seyhan S, Incesulu A, Guo S, Fitoz S, Atli EI, Gosstola NC,
877 Demir S et al. 2020. Long-range cis-regulatory elements controlling GDF6 expression are
878 essential for ear development. *The Journal of clinical investigation* **130**: 4213-4217.
879 Ball CB, Rodriguez KF, Stumpo DJ, Ribeiro-Neto F, Korach KS, Blackshear PJ, Birnbaumer L,
880 Ramos SB. 2014. The RNA-binding protein, ZFP36L2, influences ovulation and oocyte
881 maturation. *PloS one* **9**: e97324.
882 Ball CB, Solem AC, Meganck RM, Laederach A, Ramos SBV. 2017. Impact of RNA structure on
883 ZFP36L2 interaction with luteinizing hormone receptor mRNA. *RNA* **23**: 1209-1223.

884 Belloc E, Mendez R. 2008. A deadenylation negative feedback mechanism governs meiotic
885 metaphase arrest. *Nature* **452**: 1017-1021.
886 Bentley DR Balasubramanian S Swerdlow HP Smith GP Milton J Brown CG Hall KP Evers DJ
887 Barnes CL Bignell HR et al. 2008. Accurate whole human genome sequencing using
888 reversible terminator chemistry. *Nature* **456**: 53-59.
889 Bertho S, Herpin A, Branthonne A, Jouanno E, Yano A, Nicol B, Muller T, Pannetier M, Pailhoux
890 E, Miwa M et al. 2018. The unusual rainbow trout sex determination gene hijacked the
891 canonical vertebrate gonadal differentiation pathway. *Proc Natl Acad Sci U S A* **115**:
892 12781-12786.
893 Chalopin D, Volff JN, Galiana D, Anderson JL, Schartl M. 2015. Transposable elements and early
894 evolution of sex chromosomes in fish. *Chromosome Res* **23**: 545-560.
895 Chousal J, Cho K, Ramaiah M, Skarbrevik D, Mora-Castilla S, Stumpo DJ, Lykke-Andersen J,
896 Laurent LC, Blackshear PJ, Wilkinson MF et al. 2018. Chromatin Modification and Global
897 Transcriptional Silencing in the Oocyte Mediated by the mRNA Decay Activator
898 ZFP36L2. *Dev Cell* **44**: 392-402 e397.
899 Colozza G, De Robertis EM. 2014. Maternal syntabulin is required for dorsal axis formation and
900 is a germ plasm component in Xenopus. *Differentiation* **88**: 17-26.
901 Crosier PS, Kalev-Zylinska ML, Hall CJ, Flores MV, Horsfield JA, Crosier KE. 2002. Pathways
902 in blood and vessel development revealed through zebrafish genetics. *The International*
903 *journal of developmental biology* **46**: 493-502.
904 Dai S, Qi S, Wei X, Liu X, Li Y, Zhou X, Xiao H, Lu B, Wang D, Li M. 2021. Germline sexual
905 fate is determined by the antagonistic action of dmrt1 and foxl3/foxl2 in tilapia.
906 *Development (Cambridge, England)* **148**.
907 den Hollander AI, Biyanwila J, Kovach P, Bardakjian T, Traboulsi EI, Ragge NK, Schneider A,
908 Malicki J. 2010. Genetic defects of GDF6 in the zebrafish out of sight mutant and in human
909 eye developmental anomalies. *BMC genetics* **11**: 102.
910 di Clemente N, Josso N, Gouedard L, Belville C. 2003. Components of the anti-Mullerian hormone
911 signaling pathway in gonads. *Molecular and cellular endocrinology* **211**: 9-14.
912 Dobin A, Davis CA, Schlesinger F, Drenkow J, Zaleski C, Jha S, Batut P, Chaisson M, Gingeras
913 TR. 2013. STAR: ultrafast universal RNA-seq aligner. *Bioinformatics* **29**: 15-21.
914 Feron R, Zahm M, Cabau C, Klopp C, Roques C, Bouchez O, Eche C, Valiere S, Donnadieu C,
915 Haffray P et al. 2020. Characterization of a Y-specific duplication/insertion of the anti-
916 Mullerian hormone type II receptor gene based on a chromosome-scale genome assembly
917 of yellow perch, Perca flavescens. *Mol Ecol Resour* **20**: 531-543.
918 Geissler R, Scholze H, Hahn S, Streubel J, Bonas U, Behrens SE, Boch J. 2011. Transcriptional
919 activators of human genes with programmable DNA-specificity. *PloS one* **6**: e19509.
920 Goedhart J, Luijsterburg MS. 2020. VolcaNoseR is a web app for creating, exploring, labeling and
921 sharing volcano plots. *Sci Rep* **10**: 20560.
922 Gosse NJ, Baier H. 2009. An essential role for Radar (Gdf6a) in inducing dorsal fate in the
923 zebrafish retina. *Proc Natl Acad Sci U S A* **106**: 2236-2241.
924 Gramann AK, Venkatesan AM, Guerin M, Ceol CJ. 2019. Regulation of zebrafish melanocyte
925 development by ligand-dependent BMP signaling. *eLife* **8**.
926 Hall CJ, Flores MV, Davidson AJ, Crosier KE, Crosier PS. 2002. Radar is required for the
927 establishment of vascular integrity in the zebrafish. *Developmental biology* **251**: 105-117.
928 Hanel ML, Hensey C. 2006. Eye and neural defects associated with loss of GDF6. *BMC*
929 *developmental biology* **6**: 43.

930 Hartmann N, Englert C. 2012. A microinjection protocol for the generation of transgenic killifish
931 (Species: Nothobranchius furzeri). *Developmental dynamics : an official publication of the*
932 *American Association of Anatomists* **241**: 1133-1141.
933 Hattori RS, Murai Y, Oura M, Masuda S, Majhi SK, Sakamoto T, Fernandino JI, Somoza GM,
934 Yokota M, Strussmann CA. 2012. A Y-linked anti-Mullerian hormone duplication takes
935 over a critical role in sex determination. *Proc Natl Acad Sci U S A* **109**: 2955-2959.
936 Hauptmann G, Gerster T. 1994. Two-color whole-mount in situ hybridization to vertebrate and
937 Drosophila embryos. *Trends in genetics : TIG* **10**: 266.
938 Hellemans J, Mortier G, De Paepe A, Speleman F, Vandesompele J. 2007. qBase relative
939 quantification framework and software for management and automated analysis of real-
940 time quantitative PCR data. *Genome biology* **8**: R19.
941 Herpin A, Braasch I, Kraeussling M, Schmidt C, Thoma EC, Nakamura S, Tanaka M, Schartl M.
942 2010. Transcriptional rewiring of the sex determining dmrt1 gene duplicate by transposable
943 elements. *PLoS genetics* **6**: e1000844.
944 Herpin A, Schartl M. 2015. Plasticity of gene-regulatory networks controlling sex determination:
945 of masters, slaves, usual suspects, newcomers, and usurpators. *EMBO reports* **16**: 1260-
946 1274.
947 Herpin A, Schartl M, Depince A, Guiguen Y, Bobe J, Hua-Van A, Hayman ES, Octavera A,
948 Yoshizaki G, Nichols KM et al. 2021. Allelic diversification after transposable element
949 exaptation promoted gsdf as the master sex determining gene of sablefish. *Genome*
950 *research* **31**: 1366-1380.
951 Holborn MK, Einfeldt AL, Kess T, Duffy SJ, Messmer AM, Langille BL, Brachmann MK,
952 Gauthier J, Bentzen P, Knutsen TM et al. 2022. Reference genome of lumpfish Cyclopterus
953 lumpus Linnaeus provides evidence of male heterogametic sex determination through the
954 AMH pathway. *Mol Ecol Resour* **22**: 1427-1439.
955 Hollnagel A, Oehlmann V, Heymer J, Ruther U, Nordheim A. 1999. Id genes are direct targets of
956 bone morphogenetic protein induction in embryonic stem cells. *J Biol Chem* **274**: 19838-
957 19845.
958 Hudson BP, Martinez-Yamout MA, Dyson HJ, Wright PE. 2004. Recognition of the mRNA AU-
959 rich element by the zinc finger domain of TIS11d. *Nat Struct Mol Biol* **11**: 257-264.
960 Imarazene B, Du K, Beille S, Jouanno E, Feron R, Pan Q, Torres-Paz J, Lopez-Roques C, Castinel
961 A, Gil L et al. 2021. A supernumerary "B-sex" chromosome drives male sex determination
962 in the Pachon cavefish, Astyanax mexicanus. *Current biology : CB* **31**: 4800-4809 e4809.
963 Indjeian VB, Kingman GA, Jones FC, Guenther CA, Grimwood J, Schmutz J, Myers RM,
964 Kingsley DM. 2016. Evolving New Skeletal Traits by cis-Regulatory Changes in Bone
965 Morphogenetic Proteins. *Cell* **164**: 45-56.
966 Jiang L, Zhang J, Wang JJ, Wang L, Zhang L, Li G, Yang X, Ma X, Sun X, Cai J et al. 2013.
967 Sperm, but not oocyte, DNA methylome is inherited by zebrafish early embryos. *Cell* **153**:
968 773-784.
969 Jubb R. 1971. A new Nothobranchius (Pisces, Cyprinodontidae) from Southeastern Rhodesia.
970 *Journal of the American Killifish Association* **8**: 12-19.
971 Kamiya T, Kai W, Tasumi S, Oka A, Matsunaga T, Mizuno N, Fujita M, Suetake H, Suzuki S,
972 Hosoya S et al. 2012. A trans-species missense SNP in Amhr2 is associated with sex
973 determination in the tiger pufferfish, Takifugu rubripes (fugu). *PLoS genetics* **8**: e1002798.
974 Kelmer Sacramento E, Kirkpatrick JM, Mazzetto M, Baumgart M, Bartolome A, Di Sanzo S,
975 Caterino C, Sanguanini M, Papaevgeniou N, Lefaki M et al. 2020. Reduced proteasome

976 activity in the aging brain results in ribosome stoichiometry loss and aggregation. *Mol Syst*
977 *Biol* **16**: e9596.
978 Kent TV, Uzunovic J, Wright SI. 2017. Coevolution between transposable elements and
979 recombination. *Philosophical transactions of the Royal Society of London Series B,*
980 *Biological sciences* **372**: 20160458.
981 Kikuchi K, Hamaguchi S. 2013. Novel sex-determining genes in fish and sex chromosome
982 evolution. *Developmental dynamics : an official publication of the American Association*
983 *of Anatomists* **242**: 339-353.
984 Kikuchi M, Nishimura T, Ishishita S, Matsuda Y, Tanaka M. 2020. foxl3, a sexual switch in germ
985 cells, initiates two independent molecular pathways for commitment to oogenesis in
986 medaka. *Proc Natl Acad Sci U S A* **117**: 12174-12181.
987 Kikuchi M, Nishimura T, Saito D, Shigenobu S, Takada R, Gutierrez-Triana JA, Cerdan JLM,
988 Takada S, Wittbrodt J, Suyama M et al. 2019. Novel components of germline sex
989 determination acting downstream of foxl3 in medaka. *Developmental biology* **445**: 80-89.
990 Kim Y, Nam HG, Valenzano DR. 2016. The short-lived African turquoise killifish: an emerging
991 experimental model for ageing. *Dis Model Mech* **9**: 115-129.
992 Kluver N, Herpin A, Braasch I, Driessle J, Schartl M. 2009. Regulatory back-up circuit of medaka
993 Wt1 co-orthologs ensures PGC maintenance. *Developmental biology* **325**: 179-188.
994 Kluver N, Pfennig F, Pala I, Storch K, Schlieder M, Froschauer A, Gutzeit HO, Schartl M. 2007.
995 Differential expression of anti-Mullerian hormone (amh) and anti-Mullerian hormone
996 receptor type II (amhrII) in the teleost medaka. *Developmental dynamics : an official*
997 *publication of the American Association of Anatomists* **236**: 271-281.
998 Kobayashi T, Matsuda M, Kajiura-Kobayashi H, Suzuki A, Saito N, Nakamoto M, Shibata N,
999 Nagahama Y. 2004. Two DM domain genes, DMY and DMRT1, involved in testicular
1000 differentiation and development in the medaka, Oryzias latipes. *Developmental dynamics*
1001 *: an official publication of the American Association of Anatomists* **231**: 518-526.
1002 Krispin S, Stratman AN, Melick CH, Stan RV, Malinverno M, Gleklen J, Castranova D, Dejana
1003 E, Weinstein BM. 2018. Growth Differentiation Factor 6 Promotes Vascular Stability by
1004 Restraining Vascular Endothelial Growth Factor Signaling. *Arteriosclerosis, thrombosis,*
1005 *and vascular biology* **38**: 353-362.
1006 Krug J, Perner B, Albertz C, Morl H, Hopfenmuller VL, Englert C. 2023. Generation of a
1007 transparent killifish line through multiplex CRISPR/Cas9mediated gene inactivation. *eLife*
1008 **12**: e81549.
1009 Kwan KM, Fujimoto E, Grabher C, Mangum BD, Hardy ME, Campbell DS, Parant JM, Yost HJ,
1010 Kanki JP, Chien CB. 2007. The Tol2kit: a multisite gateway-based construction kit for
1011 Tol2 transposon transgenesis constructs. *Developmental dynamics : an official publication*
1012 *of the American Association of Anatomists* **236**: 3088-3099.
1013 Labun K, Montague TG, Krause M, Torres Cleuren YN, Tjeldnes H, Valen E. 2019. CHOPCHOP
1014 v3: expanding the CRISPR web toolbox beyond genome editing. *Nucleic Acids Res* **47**:
1015 W171-W174.
1016 Li L, Dong J, Yan L, Yong J, Liu X, Hu Y, Fan X, Wu X, Guo H, Wang X et al. 2017. Single-Cell
1017 RNA-Seq Analysis Maps Development of Human Germline Cells and Gonadal Niche
1018 Interactions. *Cell Stem Cell* **20**: 858-873 e854.
1019 Li M, Sun Y, Zhao J, Shi H, Zeng S, Ye K, Jiang D, Zhou L, Sun L, Tao W et al. 2015. A Tandem
1020 Duplicate of Anti-Mullerian Hormone with a Missense SNP on the Y Chromosome Is

1021 Essential for Male Sex Determination in Nile Tilapia, Oreochromis niloticus. *PLoS*
1022 *genetics* **11**: e1005678.
1023 Liao Y, Smyth GK, Shi W. 2014. featureCounts: an efficient general purpose program for
1024 assigning sequence reads to genomic features. *Bioinformatics* **30**: 923-930.
1025 Liao Y, Wang J, Jaehnig EJ, Shi Z, Zhang B. 2019. WebGestalt 2019: gene set analysis toolkit
1026 with revamped UIs and APIs. *Nucleic Acids Res* **47**: W199-W205.
1027 Liu Y, Kossack ME, McFaul ME, Christensen LN, Siebert S, Wyatt SR, Kamei CN, Horst S,
1028 Arroyo N, Drummond IA et al. 2022. Single-cell transcriptome reveals insights into the
1029 development and function of the zebrafish ovary. *eLife* **11**: e76014.
1030 Love MI, Huber W, Anders S. 2014. Moderated estimation of fold change and dispersion for RNA-
1031 seq data with DESeq2. *Genome biology* **15**: 550.
1032 Mather JP. 1980. Establishment and characterization of two distinct mouse testicular epithelial cell
1033 lines. *Biol Reprod* **23**: 243-252.
1034 Mortlock DP, Fang ZM, Chandler KJ, Hou Y, Bickford LR, de Bock CE, Eapen V, Clarke RA.
1035 2022. Transcriptional Interference Regulates the Evolutionary Development of Speech.
1036 *Genes* **13**: 1195.
1037 Mortlock DP, Guenther C, Kingsley DM. 2003. A general approach for identifying distant
1038 regulatory elements applied to the Gdf6 gene. *Genome research* **13**: 2069-2081.
1039 Myosho T, Otake H, Masuyama H, Matsuda M, Kuroki Y, Fujiyama A, Naruse K, Hamaguchi S,
1040 Sakaizumi M. 2012. Tracing the emergence of a novel sex-determining gene in medaka,
1041 Oryzias luzonensis. *Genetics* **191**: 163-170.
1042 Nishimura T, Sato T, Yamamoto Y, Watakabe I, Ohkawa Y, Suyama M, Kobayashi S, Tanaka M.
1043 2015. Sex determination. foxl3 is a germ cell-intrinsic factor involved in sperm-egg fate
1044 decision in medaka. *Science (New York, NY)* **349**: 328-331.
1045 Nishimura T, Tanaka M. 2016. The Mechanism of Germline Sex Determination in Vertebrates.
1046 *Biol Reprod* **95**: 30.
1047 Nojima H, Rothhamel S, Shimizu T, Kim CH, Yonemura S, Marlow FL, Hibi M. 2010. Syntabulin,
1048 a motor protein linker, controls dorsal determination. *Development (Cambridge, England)*
1049 **137**: 923-933.
1050 Oh D, Houston DW. 2017. Role of maternal Xenopus syntabulin in germ plasm aggregation and
1051 primordial germ cell specification. *Developmental biology* **432**: 237-247.
1052 Ortega-Recalde O, Hore TA. 2019. DNA methylation in the vertebrate germline: balancing
1053 memory and erasure. *Essays in biochemistry* **63**: 649-661.
1054 Orvis GD, Jamin SP, Kwan KM, Mishina Y, Kaartinen VM, Huang S, Roberts AB, Umans L,
1055 Huylebroeck D, Zwijsen A et al. 2008. Functional redundancy of TGF-beta family type I
1056 receptors and receptor-Smads in mediating anti-Mullerian hormone-induced Mullerian
1057 duct regression in the mouse. *Biol Reprod* **78**: 994-1001.
1058 Pan Q, Feron R, Yano A, Guyomard R, Jouanno E, Vigouroux E, Wen M, Busnel JM, Bobe J,
1059 Concordet JP et al. 2019. Identification of the master sex determining gene in Northern
1060 pike (Esox lucius) reveals restricted sex chromosome differentiation. *PLoS genetics* **15**:
1061 e1008013.
1062 Pan Q, Kay T, Depince A, Adolfi M, Schartl M, Guiguen Y, Herpin A. 2021. Evolution of master
1063 sex determiners: TGF-beta signalling pathways at regulatory crossroads. *Philosophical*
1064 *transactions of the Royal Society of London Series B, Biological sciences* **376**: 20200091.
1065 Peichel CL, McCann SR, Ross JA, Naftaly AFS, Urton JR, Cech JN, Grimwood J, Schmutz J,
1066 Myers RM, Kingsley DM et al. 2020. Assembly of the threespine stickleback Y

1067 chromosome reveals convergent signatures of sex chromosome evolution. *Genome biology*
1068 **21**: 177.
1069 Platzer M, Englert C. 2016. Nothobranchius furzeri: A Model for Aging Research and More.
1070 *Trends in genetics : TIG* **32**: 543-552.
1071 Portnoy ME, McDermott KJ, Antonellis A, Margulies EH, Prasad AB, Program NCS, Kingsley
1072 DM, Green ED, Mortlock DP. 2005. Detection of potential GDF6 regulatory elements by
1073 multispecies sequence comparisons and identification of a skeletal joint enhancer.
1074 *Genomics* **86**: 295-305.
1075 Pregizer S, Mortlock DP. 2009. Control of BMP gene expression by long-range regulatory
1076 elements. *Cytokine & growth factor reviews* **20**: 509-515.
1077 Rácz GA, Nagy N, Tóvári J, Apáti Á, Vértessy BG. 2021. Identification of new reference genes
1078 with stable expression patterns for gene expression studies using human cancer and normal
1079 cell lines. *Scientific Reports* **11**: 19459.
1080 Reed NP, Mortlock DP. 2010. Identification of a distant cis-regulatory element controlling
1081 pharyngeal arch-specific expression of zebrafish gdf6a/radar. *Developmental dynamics :*
1082 *an official publication of the American Association of Anatomists* **239**: 1047-1060.
1083 Reichwald K, Petzold A, Koch P, Downie BR, Hartmann N, Pietsch S, Baumgart M, Chalopin D,
1084 Felder M, Bens M et al. 2015. Insights into Sex Chromosome Evolution and Aging from
1085 the Genome of a Short-Lived Fish. *Cell* **163**: 1527-1538.
1086 Reuter H, Krug J, Singer P, Englert C. 2018. The African turquoise killifish Nothobranchius furzeri
1087 as a model for aging research. *Drug Discovery Today: Disease Models* **27**: 15-22.
1088 Richter A, Krug J, Englert C. 2022. Molecular Sexing of Nothobranchius furzeri Embryos and
1089 Larvae. *Cold Spring Harb Protoc* **2022**: 630-640.
1090 Settle SH, Jr., Rountree RB, Sinha A, Thacker A, Higgins K, Kingsley DM. 2003. Multiple joint
1091 and skeletal patterning defects caused by single and double mutations in the mouse Gdf6
1092 and Gdf5 genes. *Developmental biology* **254**: 116-130.
1093 Sha QQ, Yu JL, Guo JX, Dai XX, Jiang JC, Zhang YL, Yu C, Ji SY, Jiang Y, Zhang SY et al.
1094 2018. CNOT6L couples the selective degradation of maternal transcripts to meiotic cell
1095 cycle progression in mouse oocyte. *EMBO J* **37**.
1096 Sharifi-Zarchi A, Gerovska D, Adachi K, Totonchi M, Pezeshk H, Taft RJ, Scholer HR, Chitsaz
1097 H, Sadeghi M, Baharvand H et al. 2017. DNA methylation regulates discrimination of
1098 enhancers from promoters through a H3K4me1-H3K4me3 seesaw mechanism. *BMC*
1099 *Genomics* **18**: 964.
1100 Smith T, Heger A, Sudbery I. 2017. UMI-tools: modeling sequencing errors in Unique Molecular
1101 Identifiers to improve quantification accuracy. *Genome research* **27**: 491-499.
1102 Stundlova J, Hospodarska M, Luksikova K, Volenikova A, Pavlica T, Altmanova M, Richter A,
1103 Reichard M, Dalikova M, Pelikanova S et al. 2022. Sex chromosome differentiation via
1104 changes in the Y chromosome repeat landscape in African annual killifishes
1105 Nothobranchius furzeri and N. kadleci. *Chromosome Res* **30**: 309-333.
1106 Tanaka M. 2016. Germline stem cells are critical for sexual fate decision of germ cells. *Bioessays*
1107 **38**: 1227-1233.
1108 Tassabehji M, Fang ZM, Hilton EN, McGaughran J, Zhao Z, de Bock CE, Howard E, Malass M,
1109 Donnai D, Diwan A et al. 2008. Mutations in GDF6 are associated with vertebral
1110 segmentation defects in Klippel-Feil syndrome. *Human mutation* **29**: 1017-1027.

1111 Terzibasi E, Valenzano DR, Benedetti M, Roncaglia P, Cattaneo A, Domenici L, Cellerino A.
1112 2008. Large differences in aging phenotype between strains of the short-lived annual fish
1113 Nothobranchius furzeri. *PloS one* **3**: e3866.
1114 Thoma EC, Wagner TU, Weber IP, Herpin A, Fischer A, Schartl M. 2011. Ectopic expression of
1115 single transcription factors directs differentiation of a medaka spermatogonial cell line.
1116 *Stem Cells Dev* **20**: 1425-1438.
1117 Tozzini ET, Dorn A, Ng'oma E, Polacik M, Blazek R, Reichwald K, Petzold A, Watters B,
1118 Reichard M, Cellerino A. 2013. Parallel evolution of senescence in annual fishes in
1119 response to extrinsic mortality. *BMC Evol Biol* **13**: 77.
1120 Valenzano DR, Benayoun BA, Singh PP, Zhang E, Etter PD, Hu CK, Clément-Ziza M, Willemsen
1121 D, Cui R, Harel I et al. 2015. The African Turquoise Killifish Genome Provides Insights
1122 into Evolution and Genetic Architecture of Lifespan. *Cell* **163**: 1539-1554.
1123 Valenzano DR, Kirschner J, Kamber RA, Zhang E, Weber D, Cellerino A, Englert C, Platzer M,
1124 Reichwald K, Brunet A. 2009. Mapping loci associated with tail color and sex
1125 determination in the short-lived fish Nothobranchius furzeri. *Genetics* **183**: 1385-1395.
1126 Venkatesan AM, Vyas R, Gramann AK, Dresser K, Gujja S, Bhatnagar S, Chhangawala S, Gomes
1127 CBF, Xi HS, Lian CG et al. 2018. Ligand-activated BMP signaling inhibits cell
1128 differentiation and death to promote melanoma. *The Journal of clinical investigation* **128**:
1129 294-308.
1130 Wang J, Yu T, Wang Z, Ohte S, Yao RE, Zheng Z, Geng J, Cai H, Ge Y, Li Y et al. 2016. A New
1131 Subtype of Multiple Synostoses Syndrome Is Caused by a Mutation in GDF6 That
1132 Decreases Its Sensitivity to Noggin and Enhances Its Potency as a BMP Signal. *Journal of*
1133 *bone and mineral research : the official journal of the American Society for Bone and*
1134 *Mineral Research* **31**: 882-889.
1135 Wang R, Liu X, Li L, Yang M, Yong J, Zhai F, Wen L, Yan L, Qiao J, Tang F. 2022. Dissecting
1136 Human Gonadal Cell Lineage Specification and Sex Determination Using A Single-cell
1137 RNA-seq Approach. *Genomics Proteomics Bioinformatics* **20**: 223-245.
1138 Wu Q, Fukuda K, Weinstein M, Graff JM, Saga Y. 2015. SMAD2 and p38 signaling pathways act
1139 in concert to determine XY primordial germ cell fate in mice. *Development (Cambridge,*
1140 *England)* **142**: 575-586.
1141 Yang J, Li X, Li Y, Southwood M, Ye L, Long L, Al-Lamki RS, Morrell NW. 2013. Id proteins
1142 are critical downstream effectors of BMP signaling in human pulmonary arterial smooth
1143 muscle cells. *American journal of physiology Lung cellular and molecular physiology* **305**:
1144 L312-321.
1145 Yano A, Guyomard R, Nicol B, Jouanno E, Quillet E, Klopp C, Cabau C, Bouchez O, Fostier A,
1146 Guiguen Y. 2012. An immune-related gene evolved into the master sex-determining gene
1147 in rainbow trout, Oncorhynchus mykiss. *Current biology : CB* **22**: 1423-1428.
1148 Zhu A, Ibrahim JG, Love MI. 2019. Heavy-tailed prior distributions for sequence count data:
1149 removing the noise and preserving large differences. *Bioinformatics* **35**: 2084-2092.

1150

FIGURE 1

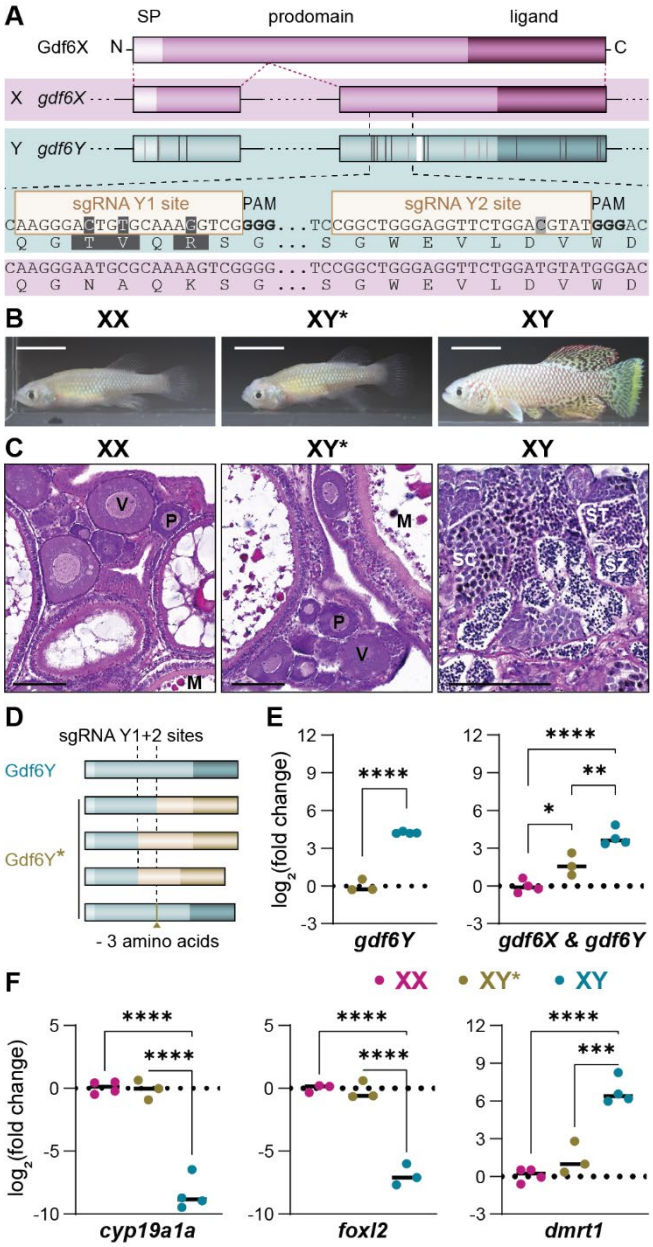
A
SP
prodomain
ligand
Gdf6X
N
C
X gdf6X
Y gdf6Y
sgRNA Y1 site
PAM
sgRNA Y2 site
PAM
CAAGGGACTGTGCAAAGGTCGGGG...TCCGGCTGGGAGGTTCTGGACGTATGGGAC
Q G T V Q R S G ... S G W E V L D V W D
CAAGGGAATGCGCAAAAGTCGGGG...TCCGGCTGGGAGGTTCTGGATGTATGGGAC
Q G N A Q K S G ... S G W E V L D V W D
B
XX
XY*
XY
C
XX
XY*
XY
V
P
M
P
V
M
ST
SC
SZ
D
sgRNA Y1+2 sites
Gdf6Y
Gdf6Y*
- 3 amino acids
E
log2(fold change)
****
gdf6Y
****
**
*
gdf6X & gdf6Y
F
XX
XY*
XY
log2(fold change)
****
****
cyp19a1a
****
****
foxl2
****
***
dmrt1

Figure 1. The inactivation of *gdf6Y* leads to full male-to-female sex reversal in *Nothobranchius furzeri*.

(A) Schematic of the Gdf6X protein domains (SP – signal peptide), the exonal distribution and comparison of the coding sequences of *gdf6X* and *gdf6Y* as well as the mutation strategy with two *gdf6Y*-specific sgRNAs that facilitate DNA double-strand breaks at a distance of 109 bp. Vertical lines in the *gdf6Y* exons indicate coding sequence differences between *gdf6X* and *gdf6Y*. SNPs: Dark gray – non-synonymous, light gray – synonymous. White – 9 bp deletion. *(B)* The phenotype of mosaic *gdf6Y*$^{-}$ animals (XY*, phenofemales) compared to an unaltered female (XX) and a wild-type male (XY) at about 3 months of age. Scale bar: 10 mm. *(C)* H&E staining of XX, XY*, and XY gonads at about 5 months of age. Oocytes: P – previtellogenic, V – vitellogenic, M – mature. SC – spermatocytes, ST – spermatids, SZ – spermatozoa. Scale bar: 100 µm. *(D)* Gdf6Y* variants that lead to full male-to-female sex reversal contain either a frameshift at one sgRNA position, a deletion between both sgRNAs, or a 9 bp deletion at the sgRNA Y2 site. *(E, F)* Expression of *gdf6X* and *gdf6Y* together and *gdf6Y* separately *(E)* as well as male and female marker genes *(F)* on mRNA-level in gonads of animals of the 1st filial generation at about 2.4 months of age. XY* – phenofemales with frameshift mutations. Statistical testing by either a two-tailed, unpaired *t*-test (*gdf6Y*) or a 1-way ANOVA and Tukey's post hoc test (others), (*) $P<0.05$, (**) $P<0.01$, (***) $P<0.001$, (****) $P<0.0001$.

FIGURE 2

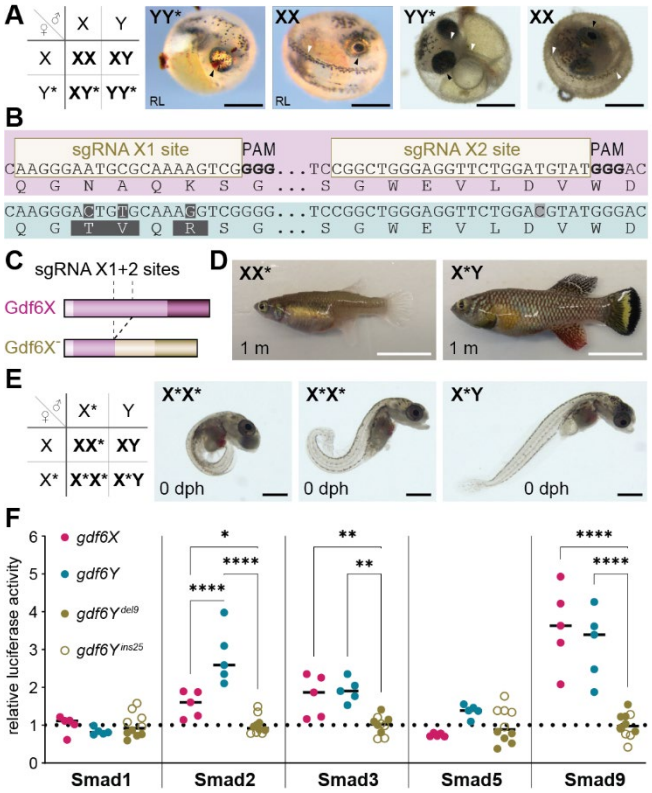
A
♀ ♂ X Y
X XX XY
Y* XY* YY*
YY*
XX
YY*
XX
RL
RL
B
sgRNA X1 site
PAM
sgRNA X2 site
PAM
CAAGGGAATGCGCAAAAGTCGGGG...TCCGGCTGGGAGGTTCTGGATGTATGGGAC
Q G N A Q K S G ... S G W E V L D V W D
CAAGGGACTGTGCAAACGTCGGGG...TCCGGCTGGGAGGTTCTGGACGTATGGGAC
Q G T V Q R S G ... S G W E V L D V W D
C
sgRNA X1+2 sites
Gdf6X
Gdf6X⁻
D
XX*
X*Y
1 m
1 m
E
♀ ♂ X* Y
X XX* XY
X* X*X* X*Y
X*X*
X*X*
X*Y
0 dph
0 dph
0 dph
F
gdf6X
gdf6Y
gdf6Y del9
gdf6Y ins25
relative luciferase activity
0
1
2
3
4
5
6
*
****
****
**
**
****
****
Smad1
Smad2
Smad3
Smad5
Smad9

Figure 2. Gdf6Y can functionally cover for Gdf6X.

(A) One quarter of the offspring from phenofemales (XY*) and males (XY) carries two Y-chromosomes (YY*), does not survive until hatching, and shows severe malformations within the egg compared to normally developed animals (here: XX at 0 dph). Shown are eggs from two different *gdf6Y*-mutants (left – *gdf6Y*$^{del6,\ del8}$, right – *gdf6Y*^{del9}). Arrows: Black – eye, white – tail. RL – reflected light microscopy. *(B)* Schematic of the *gdf6X* inactivation and *(C)* the obtained open reading frame disruption. *(D)* The phenotype of heterozygous *gdf6X*$^{-}$ females (XX*) and males (X*Y). 1 m – 1 month. *(E)* Homozygous *gdf6X*$^{-}$ (*gdf6X*^{del113}) hatchlings (X*X*; n = 15) have a detrimental curled phenotype (two manifestations shown), which prevents regular swimming behavior, while siblings (X*X, X*Y, XY; n = 34) are normal. X*Y shown for comparison. *(A, E)* Pictures of pre- or post-hatchlings acquired by brightfield microscopy if not indicated otherwise. *(A, C, E)* Scale bars: Black – 500 µm, white – 10 mm. *(F)* Luciferase reporter assay to test the differential activation of Smad1, 2, 3, 5, and 9 upon expression of *gdf6X* or *gdf6Y* compared to *gdf6Y* mutant variants (*gdf6Y*^{del9} and *gdf6Y*^{ins25}). *Gdf6Y*^{del9} has an in-frame 9 bp deletion in the prodomain's CDS, while *gdf6Y*^{ins25} harbors a 25 bp insertion at the same position leading to a frameshift and early Stop-codon. Statistical testing by a 2-way ANOVA and Holm-Šídák's multiple comparisons tests, (*) $P<0.05$, (**) $P<0.01$, (****) $P<0.0001$.

FIGURE 3

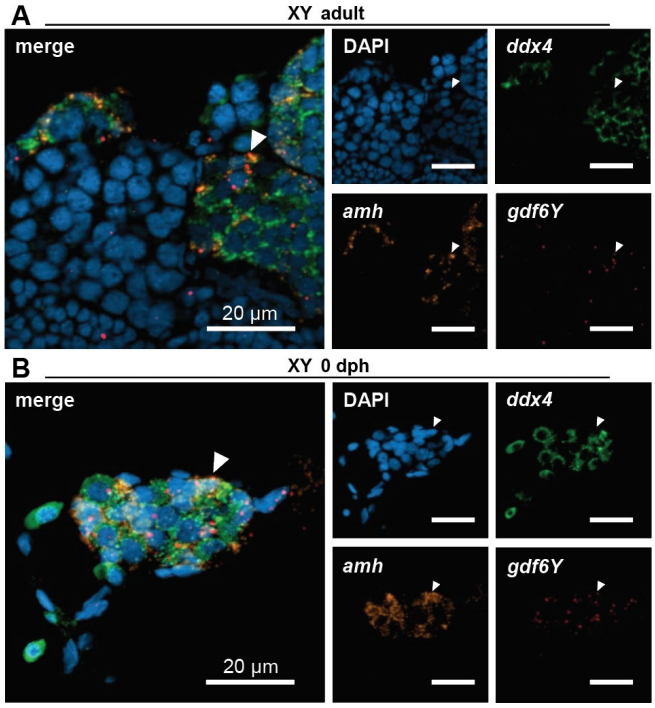

Figure 3. Localization of the gonadal *gdf6Y* expression in XY animals.

Transcripts of *gdf6Y* (red) and the GC marker *ddx4* (green) as well as the *(A)* Sertoli or *(B)* somatic supporting cell marker *amh* (orange) were detected at *(A)* adult and *(B)* 0 dph stage. *(A, B)* White arrows – cells co-expressing *gdf6Y* and *amh*.

FIGURE 4

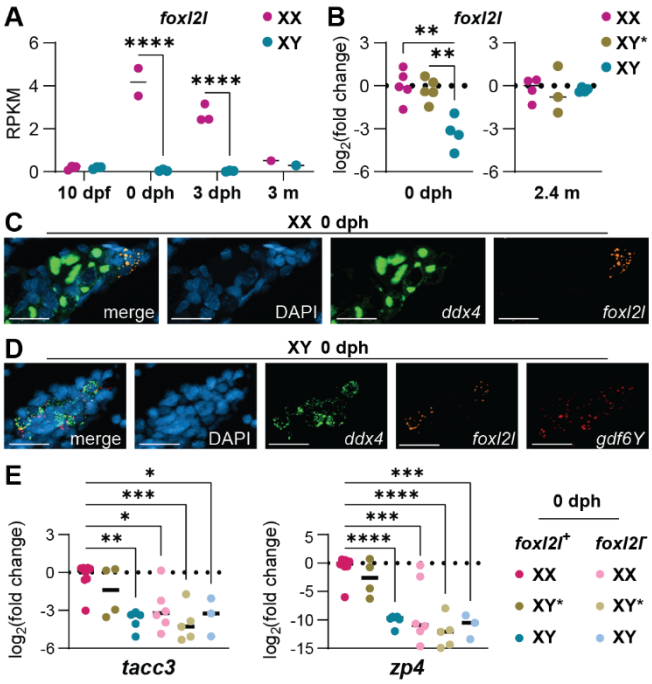

Figure 4. The *foxl2l* gene contributes to the female sex differentiation in *Nothobranchius furzeri* and is potentially repressed by *gdf6Y*.

(A) Expression analysis of *foxl2l* by RNA-Seq in the whole embryo at 10 dpf, the trunk at 0 or 3 dph, and the gonad at 3 months (m) of age in XX and XY animals. RPKM – Reads per kb of transcript per Million mapped reads. 2-way ANOVA and Šidák's post hoc test. *(B)* Expression of *foxl2l* on mRNA-level in trunks at 0 dph and adult gonads (2.4 m) of females (XX), phenofemales (XY*), and males (XY). *(C, D)* XX and XY gonadal expression at 0 dph of *foxl2l* (orange), the GC marker *ddx4* (green), and *(D) gdf6Y* (red). *(C, D)* Scale bar: 20 µm. *(E)* Expression of female marker genes on mRNA-level in trunks of females (XX), phenofemales (XY*), and males (XY) and their mosaic *foxl2l*$^{-}$ counterparts at 0 dph. *(B, E)* 1-way ANOVA and Tukey's post hoc test. *(A, B, E)* (*) $P<0.05$, (**) $P<0.01$, (***) $P<0.001$, (****) $P<0.0001$.

FIGURE 5

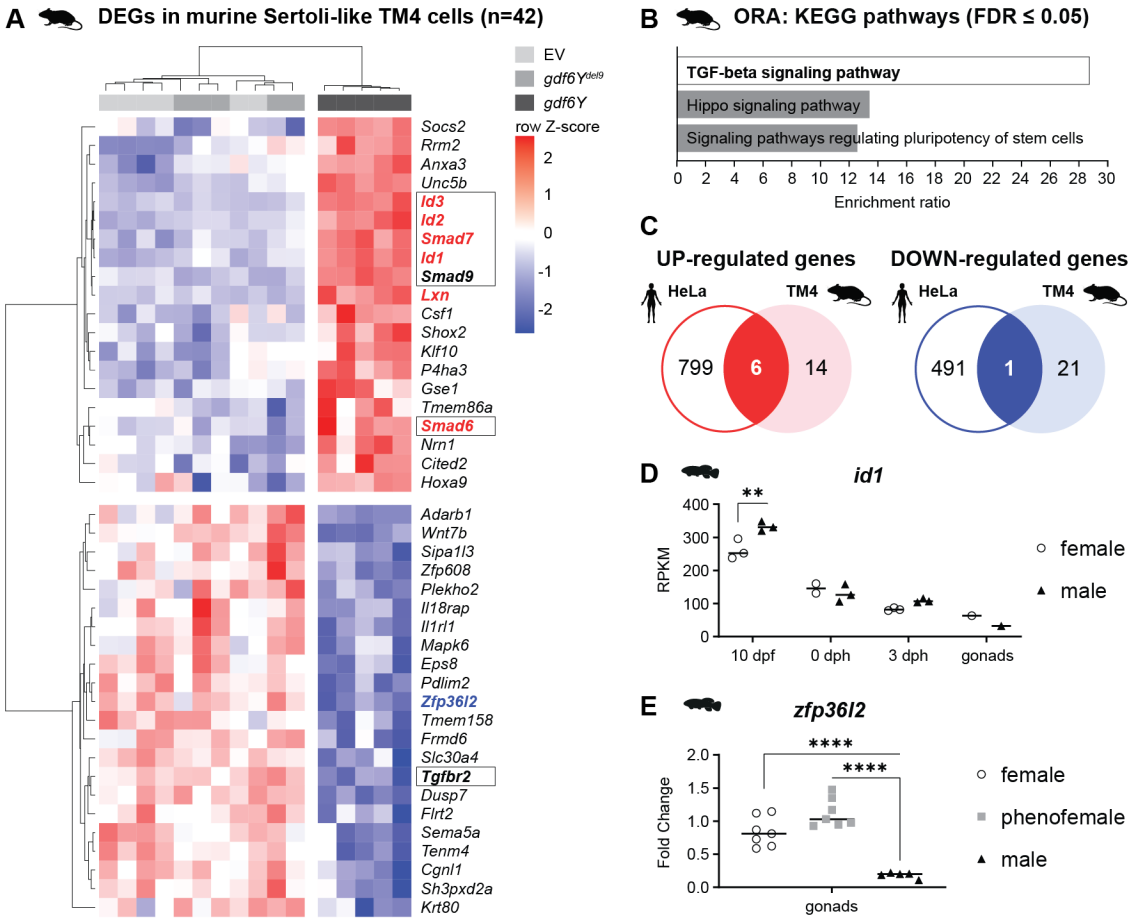
A
DEGs in murine Sertoli-like TM4 cells (n=42)
EV
gdf6Y del9
gdf6Y
row Z-score
2
1
0
-1
-2
Socs2
Rrm2
Anxa3
Unc5b
Id3
Id2
Smad7
Id1
Smad9
Lxn
Csf1
Shox2
Klf10
P4ha3
Gse1
Tmem86a
Smad6
Nrn1
Cited2
Hoxa9
Adarb1
Wnt7b
Sipa1l3
Zfp608
Plekho2
Il18rap
Il1rl1
Mapk6
Eps8
Pdlim2
Zfp36l2
Tmem158
Frmd6
Slc30a4
Tgfbr2
Dusp7
Flrt2
Sema5a
Tenm4
Cgnl1
Sh3pxd2a
Krt80
B
ORA: KEGG pathways (FDR ≤ 0.05)
TGF-beta signaling pathway
Hippo signaling pathway
Signaling pathways regulating pluripotency of stem cells
0 2 4 6 8 10 12 14 16 18 20 22 24 26 28 30
Enrichment ratio
C
UP-regulated genes
DOWN-regulated genes
HeLa
TM4
799
6
14
HeLa
TM4
491
1
21
D
id1
RPKM
400
300
200
100
0
**
10 dpf
0 dph
3 dph
gonads
female
male
E
zfp36l2
Fold Change
2.0
1.5
1.0
0.5
0.0
****
****
gonads
female
phenofemale
male

Figure 5. Gdf6Y leads to the specific regulation of certain genes independent of the targeted cell's identity.

(A) Heatmap of DEGs between murine Sertoli-like TM4 cells transfected with a *gdf6Y* expression plasmid and TM4 cells transfected with either a *gdf6Y* mutant variant (*gdf6Y*^{del9}) expression plasmid or an empty vector (EV). *(B)* Overrepresentation analysis (ORA) of KEGG pathways within the 42 DEGs identified in TM4 cells. Genes of the "TGF-beta signaling pathway" are boxed and highlighted in bold letters in *(A)*. FDR – false discovery rate. *(C)* Overlap of the up- or downregulated DEGs identified in TM4 cells with those identified in human HeLa cells. The common genes are highlighted in red (upregulated genes) or blue (the downregulated gene) in *(A)*. *(D)* The expression of *id1* derived from RNA-Seq data in whole embryos at 10 dpf, embryo trunks at 0 or 3 dph, and gonads at 3 months of age in female and male *N. furzeri*. 2-way ANOVA and Šídák's multiple comparisons test between females and males. (**) $P<0.01$. *(E)* RT-qPCR analysis of the *zfp36l2* expression in *N. furzeri* gonads of 3 months old females, males, and phenofemales carrying the *gdf6Y*^{del9} mutation. 1-way ANOVA and Dunnett's multiple comparisons test with males, (****) $P<0.0001$.

SUPPLEMENTAL FIGURE S1

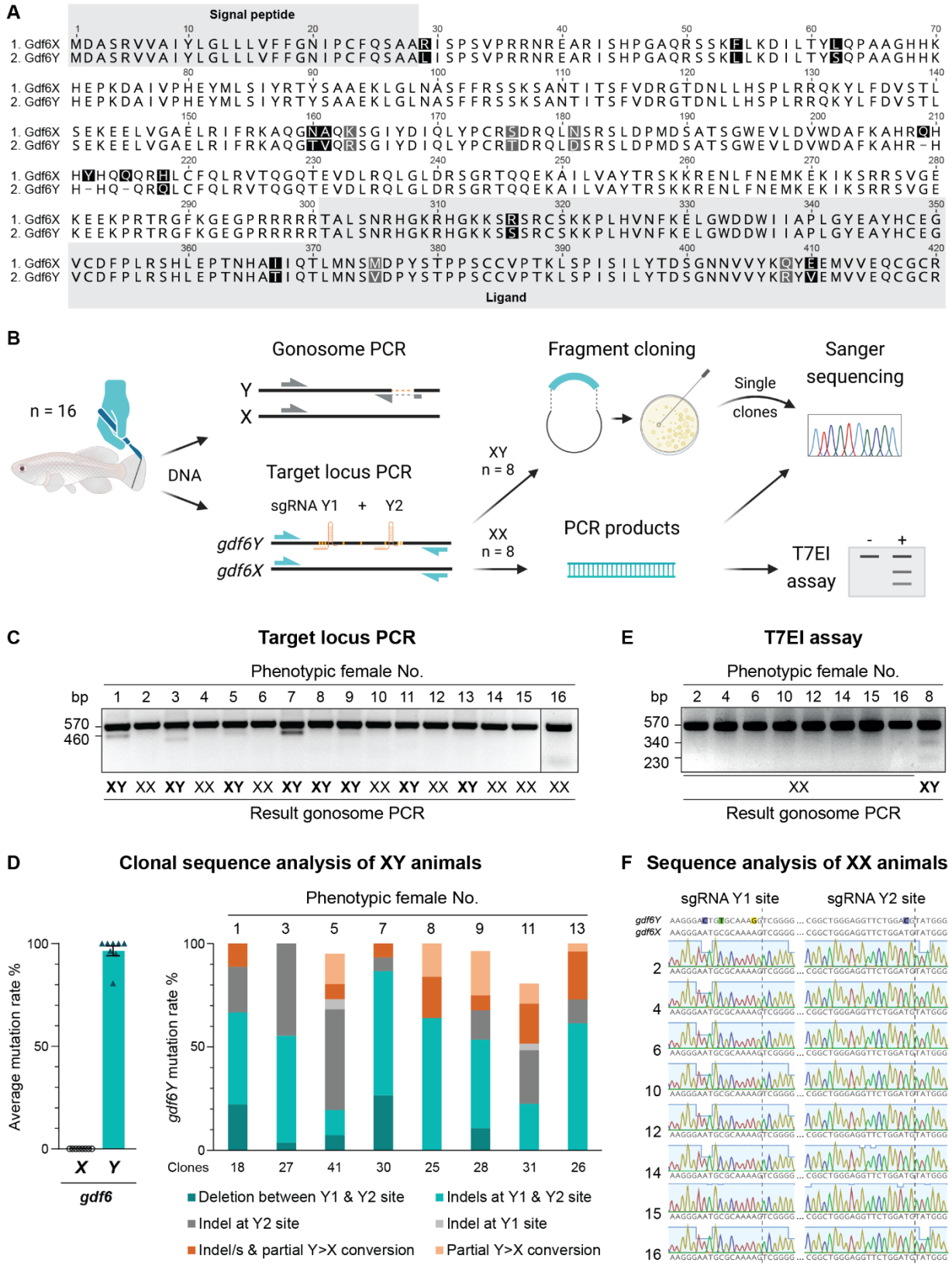

Supplemental Figure S1. Comparison of Gdf6X and Gdf6Y and analysis of mosaic *gdf6Y* mutants.

(A) Alignment of 1. Gdf6X and 2. Gdf6Y amino acid sequences (one-letter code). Sequence differences are highlighted in gray for similar and black for dissimilar amino acids. *(B)* Schematic of *gdf6Y* mutant analysis (Created with BioRender.com). T7EI – T7 endonuclease I. *(C)* Ethidium bromide-stained agarose gel picture of the sgRNA Y1 and Y2 target locus PCR on fin tissue lysates from the 16 phenotypically female CRISPR/Cas9-mutated animals. The sex chromosomes of each individual, as derived from the gonosome PCR, are indicated below the samples. *(D)* Result of the clonal sequence analysis of the 8 CRISPR/Cas9-mutated XY animals. Left: Average mutation rates in *gdf6X* and *gdf6Y* with SEM and individual values. Right: *Gdf6Y* mutation rates in the individual animal samples are separated into the different observed mutation types. Apart from insertion and deletion (indel) events at either or both sgRNA target sites, partial gene conversion between *gdf6X* and *gdf6Y* was observed probably due to homology-directed repair of DNA double-strand breaks. *(E)* Ethidium bromide-stained agarose gel picture of the T7EI assay on target locus PCR products from the 8 CRISPR/Cas9-mutated XX animals. No mutations were detected compared to the CRISPR/Cas9-mutated XY animal sample. *(F)* Partial sequence alignments with chromatograms of target locus PCR products from the 8 CRISPR/Cas9-mutated XX animals. No double peaks or decreased sequence qualities (light blue columns) were detected in chromatograms at the putative Cas9 cleavage sites mediated by sgRNA Y1 and Y2 (dashed lines).

SUPPLEMENTAL FIGURE S2

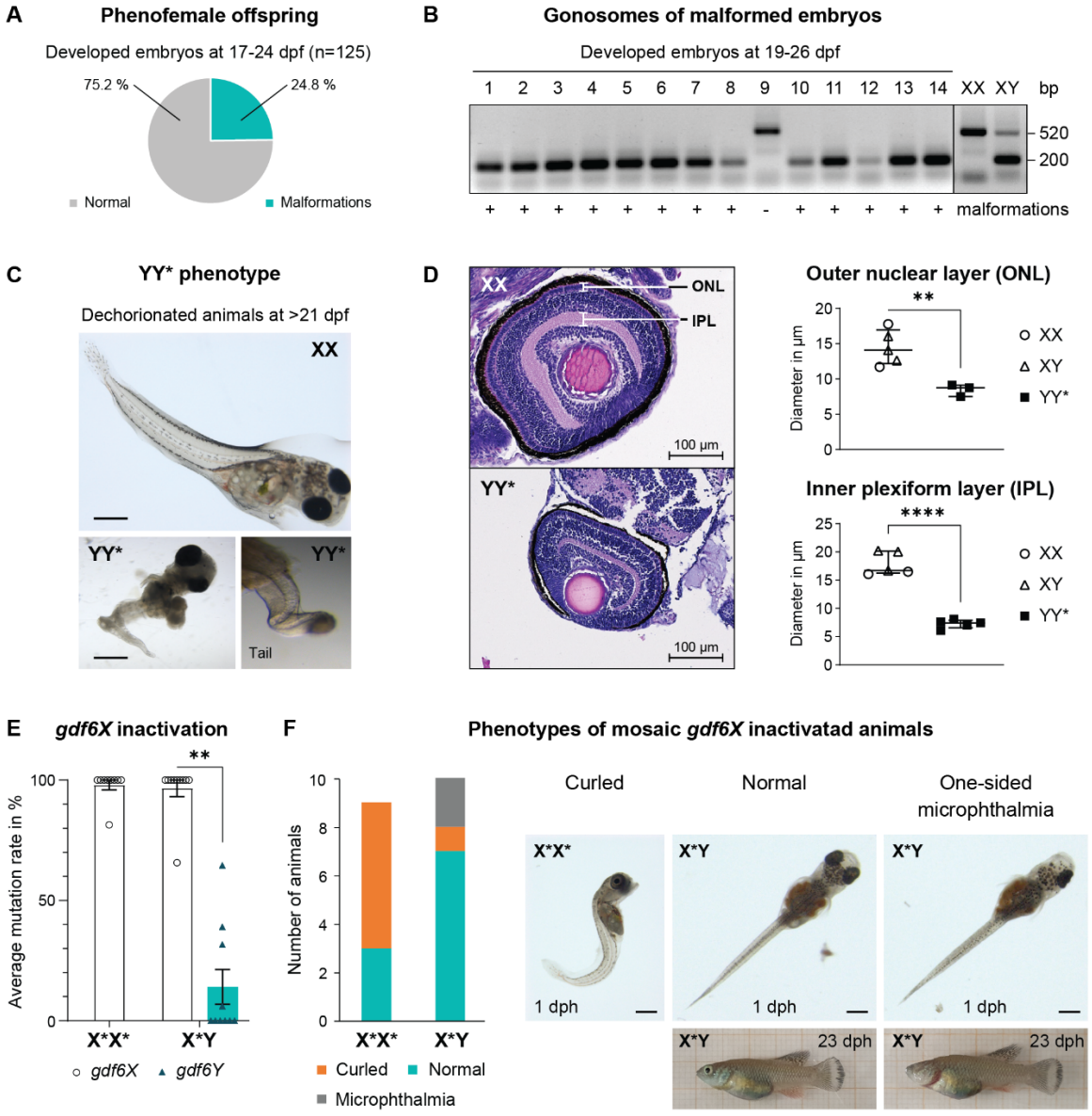

Supplemental Figure S2. YY* embryo and *gdf6X* mutant phenotypes.

(A) One quarter of a phenofemale's (*gdf6Y*^{del9}) offspring develops malformations. *(B)* Ethidium bromide-stained agarose gel picture of a molecular sexing assay utilizing an amplicon length polymorphism between the X and Y chromosomes. In malformed embryos, only the Y-chromosomal fragment was detected indicating their identity as YY* embryos (*gdf6Y*$^{del6,\ del8}$). *(C)* Dechorionated YY* embryos (*gdf6Y*^{del113}) have unpigmented and malformed tails as well as smaller eyes than normally developing e.g., XX, animals at 0 dph. *(D)* Left: H&E staining of normally developed (XX) and underdeveloped YY* (*gdf6Y*$^{del6,\ del8}$) eyes at 0 dph or 19-26 dpf, respectively. Right: Quantification of diameters (median with interquartile range) of the outer nuclear layer (ONL) and the inner plexiform layer (IPL) of the retinas of normally developed and YY* (*gdf6Y*$^{del6,\ del8}$) animals. The ONL consists of the photoreceptor cell bodies and the IPL contains the synapses between the bipolar cell axons and the dendrites of the ganglion and amacrine cells. Layer diameter was measured at three different positions per sample using ZEN 2.6 (Blue Edition, Zeiss) and averaged. Statistical testing by a two-tailed, unpaired *t*-test. *(E)* Result of the sequence analysis with the Synthego ICE tool (v3.0) of the 19 *gdf6X*-mosaic animals created with CRISPR/Cas9. Statistical testing by a Wilcoxon matched-pairs signed rank test corrected for multiple testing with the Holm-Šídák method. *(F)* Distribution according to gonosomes and representation of the phenotypes of *gdf6X*-mosaic animals. Predominantly females (X*X*) had a detrimental curled phenotype, while one-sided microphthalmia was present only in two males (X*Y). *(G) Gdf6X*/*gdf6Y* double mutant hatchlings (X*Y*; n = 30) have a detrimental curled phenotype (two manifestations shown), which prevents regular swimming behavior, while siblings (XX*, XY; n = 59) are normal in this regard. XX* shown for comparison. *(C, F, G)* Scale bars: 500 µm. *(H)* Schematic of the chromosomal location and expression of *pctp* and *rnf19a* in trunks

of XX, XY*, XY, and YY* embryos at 11 dpf. SDR – sex-determining region. Sgr05 – synteny group 5. Statistical testing by a 1-way ANOVA and Tukey's post hoc test. *(D, E, H)* (**) $P<0.01$, (***) $P<0.001$, (****) $P<0.0001$.

SUPPLEMENTAL FIGURE S3

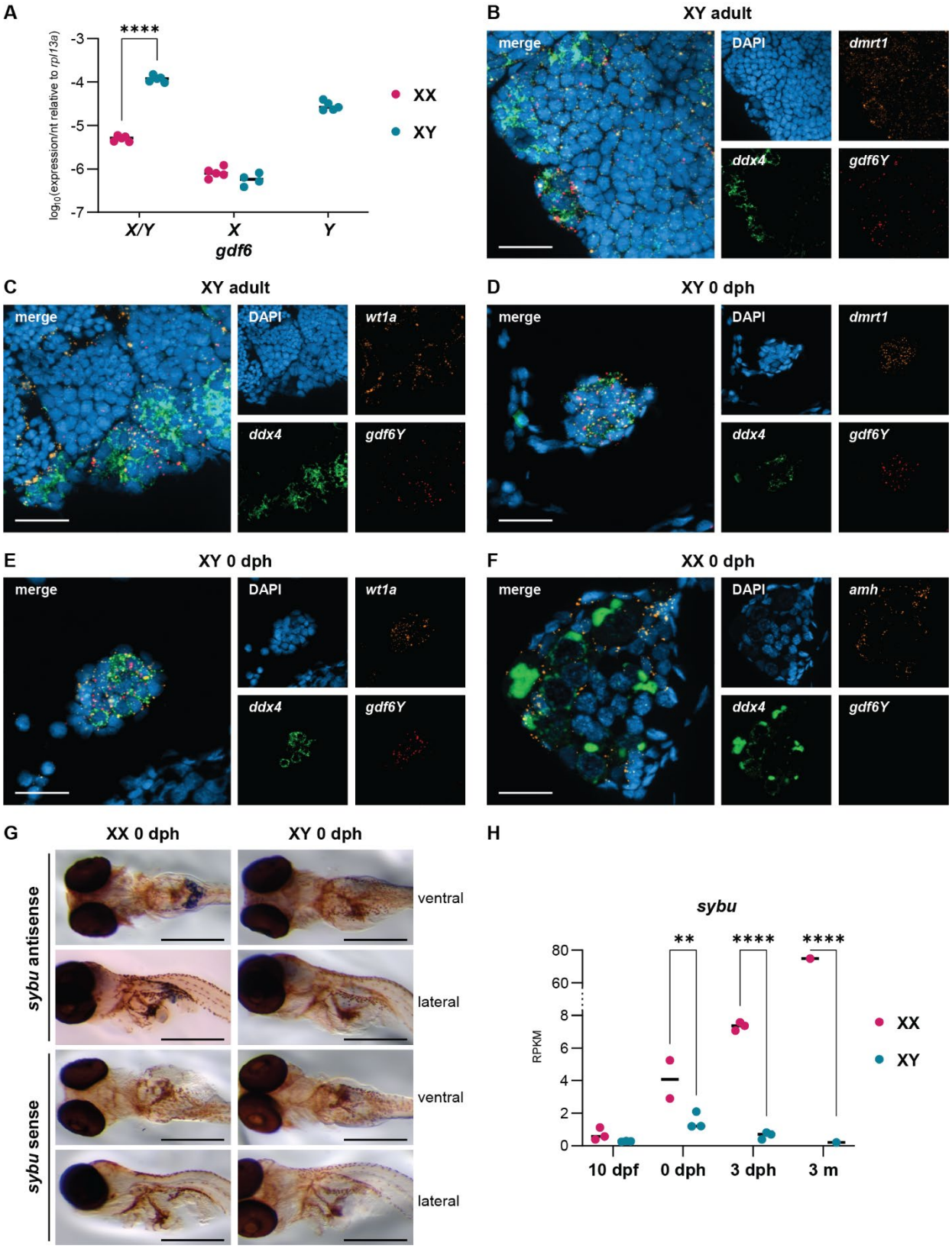

Supplemental Figure S3. *Gdf6Y* expression in *N. furzeri.*

(A) Expression of *gdf6X* and *gdf6Y* together and separately relative to *rpl13a* in gonads of adult females (XX) and males (XY). *(B, C, D, E, F)* Transcripts of *gdf6Y* (red) and the GC marker *ddx4* (green) as well as one somatic cell marker were detected. Scale bars: 20 µm. The somatic cell markers *dmrt1 (B, D)* and *wt1a (C, E)* were detected in the testes of adult *(B, C)* and 0 dph animals *(D, E)*. *(F)* The somatic cell marker *amh* (orange) was detected in a 0 dph ovary. *(G)* Whole mount *in situ* hybridization of MZM0403 hatchlings with *sybu*-mRNA antisense (females: n = 5, males: n = 3) and sense probes (n = 8; definitive females: n = 3, definitive males: n = 3). *(H)* Expression analysis of *sybu* by RNA-Seq in the whole embryo at 10 dpf, the trunk at 0 or 3 dph, and the gonad at 3 months (m) of age in XX and XY animals. RPKM – Reads per kb of transcript per Million mapped reads. *(A, H)* Statistical testing by a 2-way ANOVA and Šidák's post hoc test between XX and XY, (**) $P<0.01$, (****) $P<0.0001$.

SUPPLEMENTAL FIGURE S4

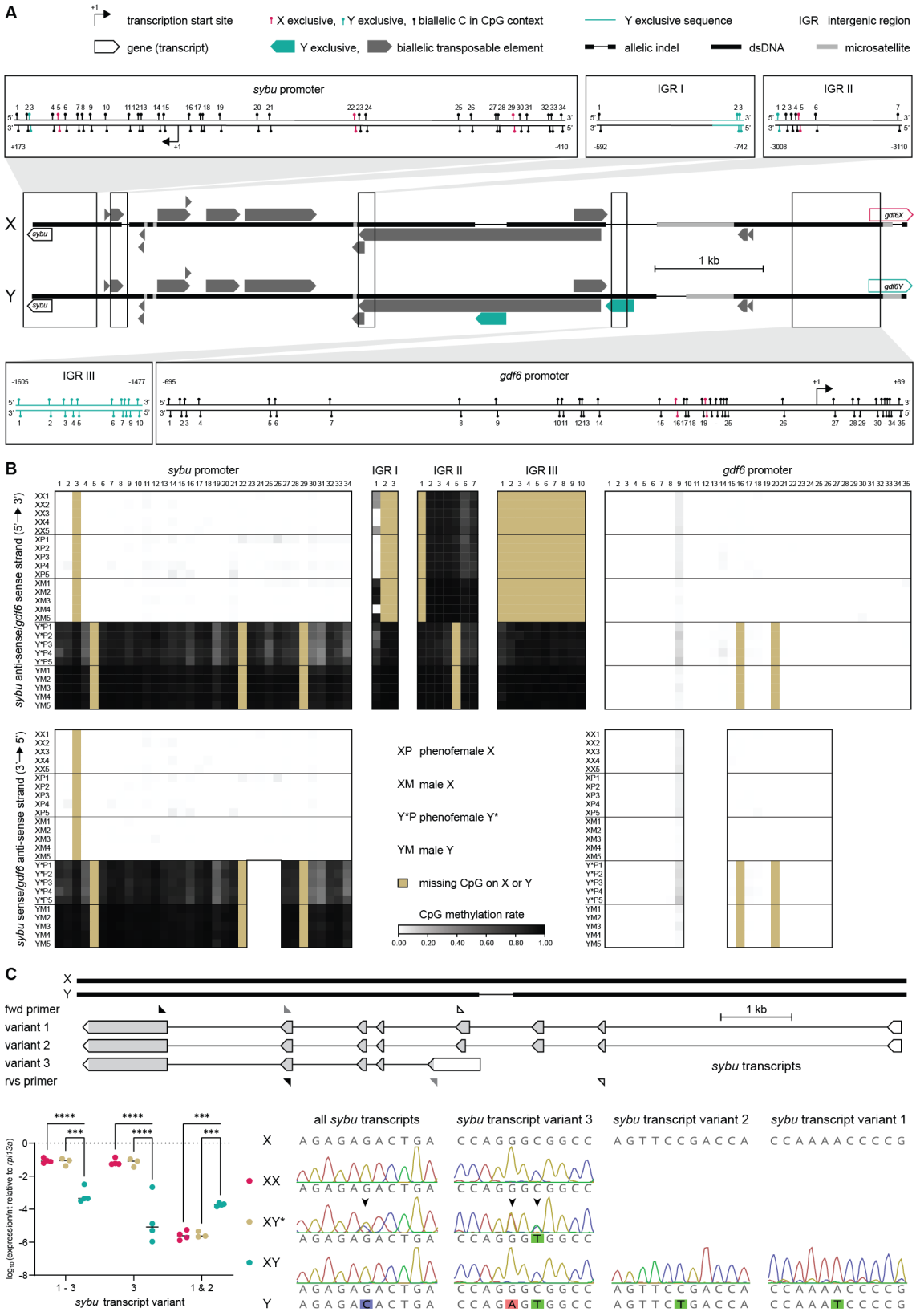

Supplemental Figure S4. DNA methylation of the genomic region between *sybu* and *gdf6X/Y* on the sex chromosomes in gonads.

(A) Schematic of the analyzed region of the X and Y chromosome containing Y exclusive TEs (*gdf6Y*-distal TE: NfRep007207 of unknown identity; *gdf6Y*-proximal TE: partial retrotransposon NfRep000041 of LINE/RTE-BovB type; source: https://nfingb.leibniz-fli.de). Insets show the CpG positions of the analyzed subregions. *(B)* Heatmaps of CpG methylation rates on the X and Y chromosomes in the gonads of the analyzed individuals (n=5). For some locations, the *sybu* sense strand (bottom panels) was analyzed in addition to the *gdf6X/Y* sense strand (upper panels). *(C)* Schematic and sex-specific expression of three different *sybu* transcripts in the gonads of females (XX), phenofemales (XY*), and males (XY). Exons and transcript-specific primer pairs are indicated with triangles (black – transcript variants 1-3, gray – variant 3, white – variant 1 and 2). *Sybu* cDNA sequences indicate an X-exclusive transcription in males, while expression from the Y chromosome is reactivated in phenofemales. Statistical testing by a 2-way ANOVA and Tukey's post hoc test, (***) $P<0.001$, (****) $P<0.0001$.

SUPPLEMENTAL FIGURE S5

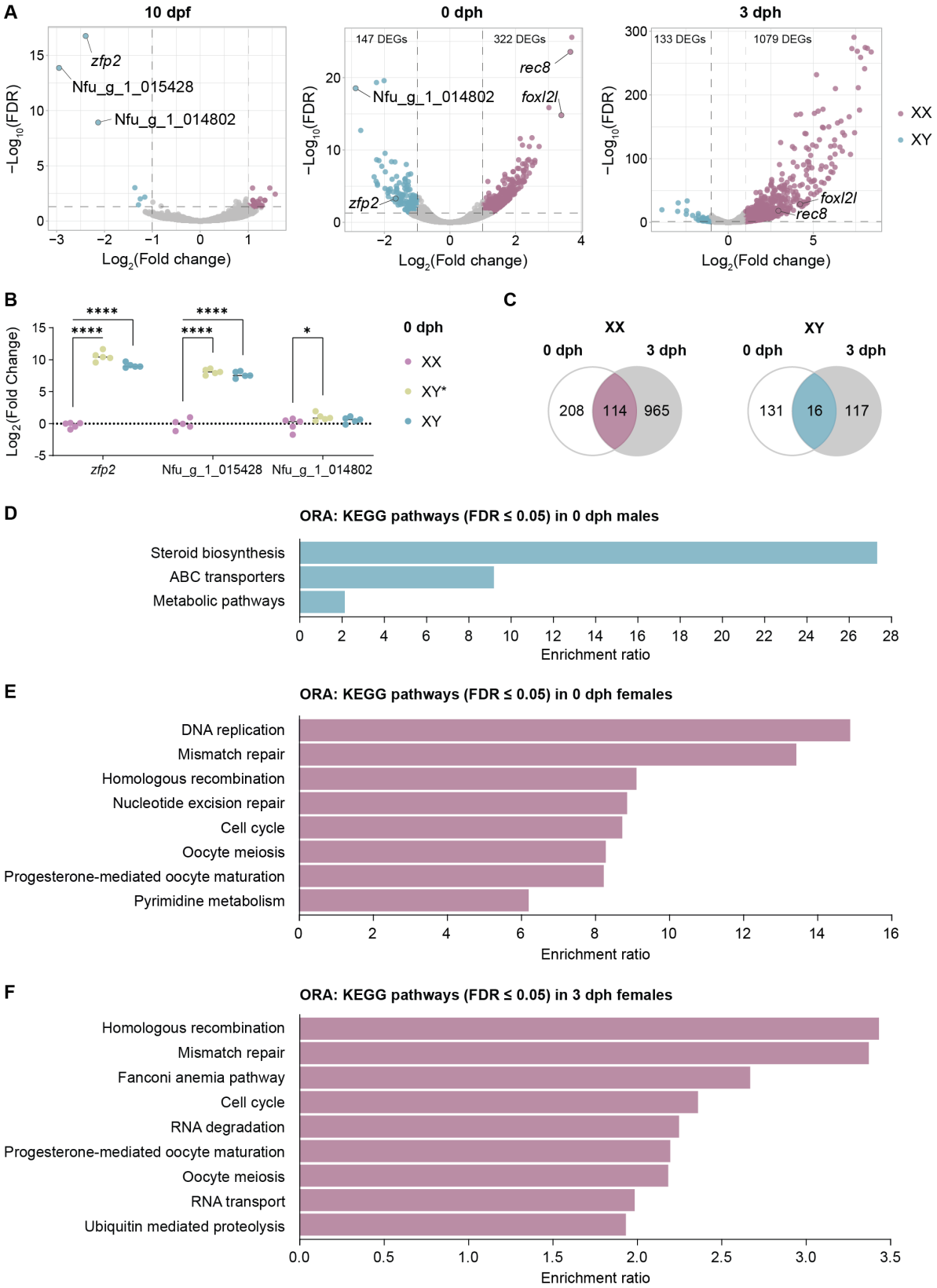

Supplemental Figure S5. RNA-Seq results show that ovarian development starts before 0 dph in *N. furzeri.*

(A) Volcano plots of DEGs between XX and XY animals in the whole embryo at 10 dpf and in trunk parts at 0 and 3 dph as derived from a respective previously published data set (XX at 0 dph n=2, others n=3; Reichwald et al. 2015). *(B)* Expression of the three top DEGs at 10 dpf in trunks of XX, XY*, and XY animals at 0 dph. Statistical testing by a 1-way ANOVA and Dunnett's multiple comparisons test with XX animals, (*) $P<0.05$, (****) $P<0.0001$. *(C)* Overlap of female and male DEGs between 0 and 3 dph. *(D, E, F)* Overrepresentation analysis (ORA) of KEGG pathways within the male- *(D)* and female-specific *(E)* DEGs at 0 dph as well as the female-specific *(F)* DEGs at 3 dph.

SUPPLEMENTAL FIGURE S6

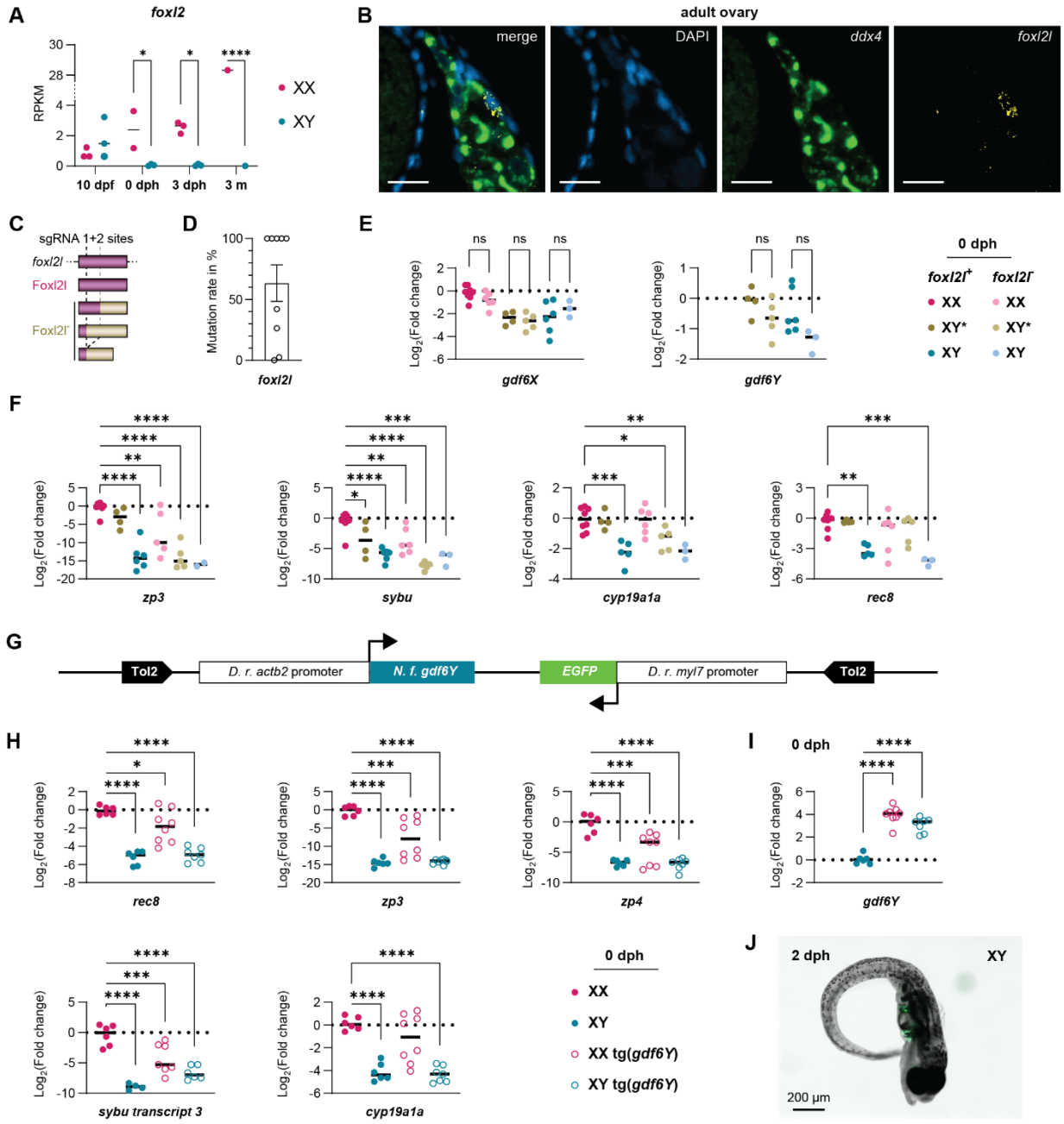

Supplemental Figure S6. Expression of oogenesis-associated genes in mosaic *foxl2l*-mutants and *gdf6Y*-transgenic animals.

(A) Expression analysis of *foxl2* by RNA-Seq in the whole embryo at 10 dpf, the trunk at 0 or 3 dph, and the gonad at 3 months (m) of age in XX and XY animals. 2-way ANOVA and Šidák's post hoc test. *(B)* Ovarian expression at 5 weeks of age of *foxl2* (yellow) and the GC marker *ddx4* (green). Nuclei are stained with 4′,6-Diamidin-2-phenylindol (DAPI, blue). Scale bar: 20 µm. *(C)* Frameshifts induced by one or both *foxl2l* sgRNAs lead to truncated Foxl2l-proteins (Foxl2l^{-}). *(D)* Result of sequence analyses with the Synthego ICE tool (v3.0) of the 9 *foxl2l*-mosaic animals created with CRISPR/Cas9. *(E)* Expression of *gdf6X* and *gdf6Y* in trunks of females (XX), phenofemales (XY*), and males (XY) and their mosaic *foxl2l*$^{-}$ counterparts at 0 dph. Statistical testing by a 1-way ANOVA and Holm-Šídák's multiple comparisons tests. *(F)* Expression of female marker genes in trunks of females, phenofemales, and males and their mosaic *foxl2l*$^{-}$ counterparts at 0 dph. *(G)* Schematic of Tol2-transgene to drive ubiquitous *gdf6Y*-expression with a *D. rerio* (*D. r.*) *actb2* promoter in *N. furzeri* (*N. f.*). Heart-specific *EGFP expression* by a *D. r. myl7* promoter is used as a selection marker. *(H)* Expression of female marker genes in trunks of females, males, and their mosaic *gdf6Y*-transgenic (tg(*gdf6Y*)) counterparts at 0 dph. *(F, H)* Statistical testing by a 1-way ANOVA and Dunnett's multiple comparisons test with XX animals. *(I)* Expression of *gdf6Y* in trunks of females, males, and their mosaic *gdf6Y*-transgenic counterparts at 0 dph. Statistical testing by a 1-way ANOVA and Dunnett's multiple comparisons test with XY animals. *(E, F, H, I)* (*) $P<0.05$, (**) $P<0.01$, (***) $P<0.001$, (****) $P<0.0001$. *(J)* Curled *gdf6Y*-transgenic XY-larva with heart-specific EGFP expression (green).

SUPPLEMENTAL FIGURE S7

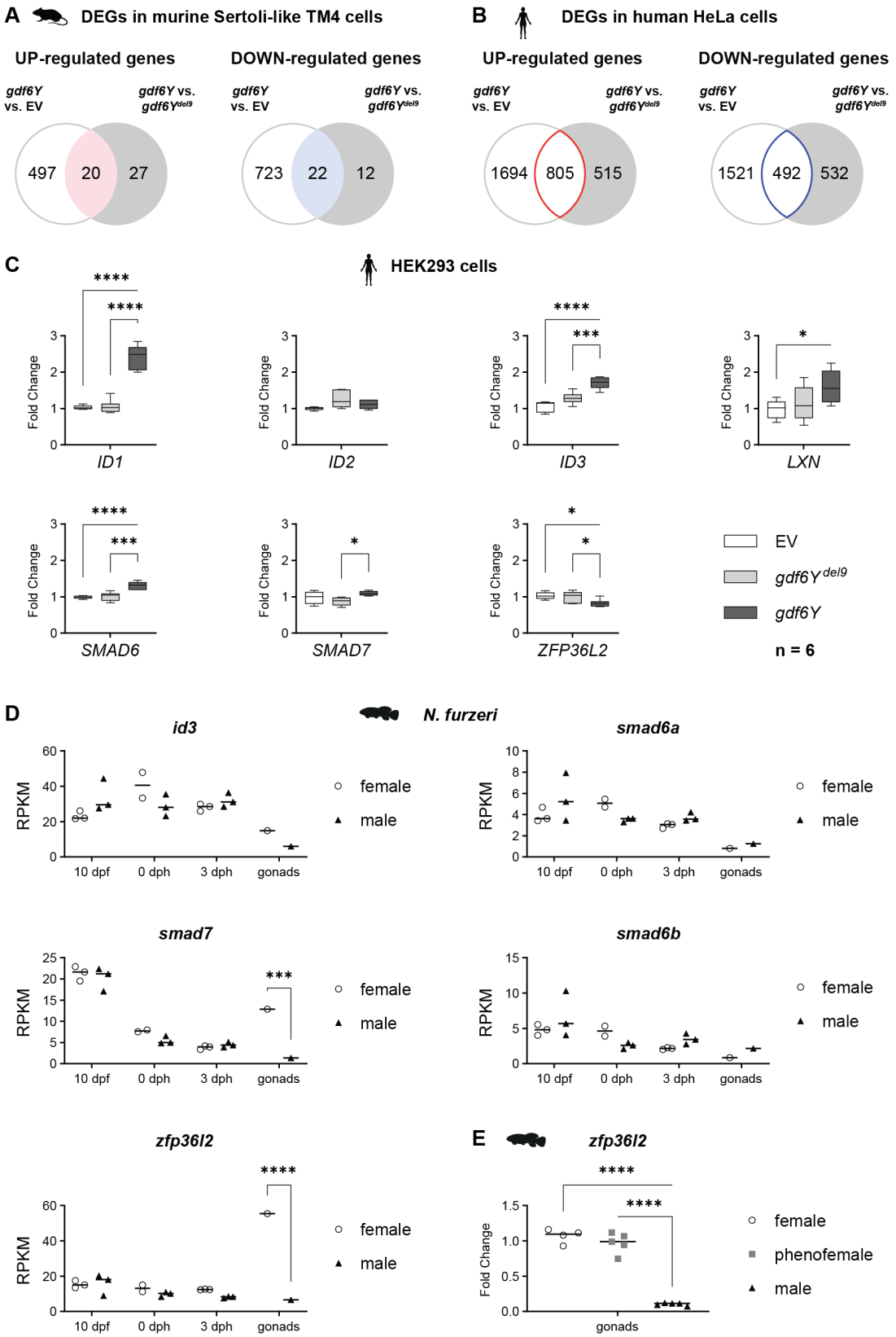

Supplemental Figure S7. Gdf6Y-responsive genes in different cell lines and *N. furzeri*.

(A) Overlap of the up- or downregulated DEGs between murine Sertoli-like TM4 cells transfected with either a *gdf6Y* or a *gdf6Y* mutant variant (*gdf6Y*^{del9}) expression plasmid and TM4 cells transfected with either a *gdf6Y* expression plasmid or an empty vector (EV). *(B)* Overlap of the up- or downregulated DEGs between human HeLa cells transfected with either a *gdf6Y* or a *gdf6Y* mutant variant (*gdf6Y*^{del9}) expression plasmid and TM4 cells transfected with either a *gdf6Y* expression plasmid or an empty vector (EV). *(C)* RT-qPCR analysis of the genes commonly up- or downregulated in TM4 and HeLa cells in human HEK293 cells transfected with an expression plasmid for *gdf6Y* or a *gdf6Y* mutant variant (*gdf6Y*^{del9}) or an empty vector (EV). 1-way ANOVA and Dunnett's multiple comparisons test with the *gdf6Y* transfected cells. *(D)* The expression of *id3*, *smad6a*, *smad6b*, *smad7*, and *zfp36l2* derived from RNA-Seq data in whole embryos at 10 dpf, embryo trunks at 0 or 3 dph and gonads at 3 months of age in female and male *N. furzeri*. 2-way ANOVA and Šídák's multiple comparisons test between females and males. *(E)* RT-qPCR analysis of the *zfp36l2* expression in *N. furzeri* gonads of 3 months old females, males, and phenofemales carrying the frameshift mutation *gdf6Y*^{del113}. 1-way ANOVA and Dunnett's multiple comparisons test with males. *(C, D, E)* (*) $P<0.05$, (***) $P<0.001$, (****) $P<0.0001$.

SUPPLEMENTAL TABLES

Supplemental Table S1. Mutations of *gdf6Y* and *gdf6X* used in this work. (*) Artificial mutation used in *in vitro* analysis.

Name	Sequence at Cas9 cleavage site (|) with		Figure
	sgRNA X/Y 1	sgRNA X/Y 2	
gdf6Y	**AAAGG|TCGGGG**	**GGTTCTGGACG| TATGGGACGCG**	**wild-type**
gdf6Y$^{del4,\ ins3}$	AAAGG|----GG	GGTTCTGGACG| CGTTATGGGACGCG	1E, F; 4B 2.4 m; S4C
gdf6Y$^{del4,\ ins13}$	AAAGG|----GG	GGTTCTGGACG| CGTTAAGTCTGATTATGGGACGCG	
gdf6Y^{del4}	AAAGG|TCGGGG	GGATATGG---| -ATGGGACGCG	
gdf6Y$^{del6,\ del8}$	AA---|---GGG	GGT--------| TATGGGACGCG	2A; S2B, D
gdf6Y^{del9}	AAAGG|TCGGGG	GGTTCTGGACG| ---------CG	2A, F; 4E; 5A, C, E; S2A, G, H; S5B; S6C-F; S7A-C
gdf6Y^{del113}	AAAGG|------	----------| ----GGACGCG	4B 0 dph; S2C; S4B; S7E
(*) *gdf6Y*^{ins25}	AAAGG|TCGGGG	GGTTCTGGACG|CGTTTAAAGCACATCGGCTGGGAGGTTCTGGACGCG	2F
gdf6X	**AAAAG|TCGGGG**	**GGTTCTGGATG| TATGGGACGCG**	**wild-type**
gdf6X^{del113}	AAA--|------	----------| --TGGGACGCG	2D, E

Supplemental Table S2. Oligonucleotides used for the synthesis of sgRNA *in vitro* transcription templates.

Name	Sequence (sgRNA target bold)	Application
sgRNA_Gdf6_2_fw	TAGG**AAGGGACTGTGCAAAGGTCG**	Cloning of sgRNA Y1
sgRNA_Gdf6_2_rv	AAAC**CGACCTTTGCACAGTCCCTT**	
sgRNA_Gdf6_4_fw	TAGG**CGGCTGGGAGGTTCTGGACGTAT**	Cloning of sgRNA Y2
sgRNA_Gdf6_4_rv	AAAC**ATACGTCCAGAACCTCCCAGCCG**	
T7sgRgdf6X1F	GAAATTAATACGACTCACTATAGG**AAGGGAATGCGCAAAAGTCG** GTTTTAGAGCTAGAAATAG	Amplification of sgRNA X1
T7sgRgdf6X2F	GAAATTAATACGACTCACTATAGG**CGGCTGGGAGGTTCTGGATGTAT** GTTTTAGAGCTAGAAATAG	Amplification of sgRNA X2
T7sgRfoxl2l2F	GAAATTAATACGACTCACTATAGG**GAAGCCCCCCTATTCCTACG** GTTTTAGAGCTAGAAATAG	Template for *foxl2l*-sgRNA1
T7sgRfoxl2l3F	GAAATTAATACGACTCACTATAGG**AAGGTGCCCCGAGAGCGCGG** GTTTTAGAGCTAGAAATAG	Template for *foxl2l*-sgRNA2
sgRNAR	AAAAGCACCGACTCGGTGCCACTTTTTCAAGTTGATAACGGACTAGC CTTATTTTAACTTGCTATTTCTAGCTCTAAAAC	Template for sgRNAs
T7F	GAAATTAATACGACTCAC	Amplification sgRNAs
pDRrvs	AAAAGCACCGACTCGGTGC	

Supplemental Table S3. RNAscope probes purchased from Advanced Cell Diagnostics.

Name	Targeted transcript (NCBI Reference Sequence)	Catalogue-No.
RNAscope® Probe - Nf-ddx4	XM_015957842.1 (*ddx4*)	563361
RNAscope® Probe - Nf-amh-C2	XM_015977279.1 (*amh*)	830891-C2
RNAscope® Probe - Nf-LOC107386104-C2	XM_015960292.1 (*dmrt1*)	830901-C2
RNAscope® Probe - Nf-LOC107389222-C2	XM_015965254.1 (*wt1a*)	830871-C2
RNAscope® Probe - Nf-LOC107390636-C2	XM_015967458.1 (*foxl2l*)	831201-C2
RNAscope® Probe - Nf-gdf6y-C3	*gdf6Y*-transcript (Reichwald et al. 2015)	563381-C3

Supplemental Table S4. Oligonucleotides used for RT-qPCR.

Name	Sequence	Usage
qRPL13a_ex4/5_fw	ACTGTCAGAGGCATGCTTCC	Quantification of *rpl13a* as universal *N. furzeri* reference gene
qRPL13a_ex6_rv	GGCGCACAATTTTCAGAGCA	
eef1a1l1F	GAAGGAAGCCGCCGAGATG	Quantification of *eef1a1l1* as 2nd *N. furzeri* reference gene (Fig. 4E *tacc3*; S6F *cyp19a1a*, *rec8*; S6H, I)
eef1a1l1R	CAATGATGGTCACGTAGTACTTG	
cyp19a1aqF1	TTGGGATGCATGAGAGAGGC	Quantification of *cyp19a1a* in adult *N. furzeri* gonads
cyp19a1aqR1	GAGTCTGTGTGGAGGAGATGC	
cyp19a1aF2	GCAGATCTCATATTTGCACAAAACC	Quantification of *cyp19a1a* in *N. furzeri* trunks at 0 dph
cyp19a1aR2	CGTTCTGAAGCTCTTCTCCTAC	
dmrt1ex3qF1	CTGTGGAAGGACGTTCCAGC	Quantification of *dmrt1* in *N. furzeri*
dmrt1ex4qR1	GTCTCCAGCAGCAGGTCAG	
foxl2-qRTF	GGTCCAGGAGAAAGTCACGG	Quantification of *foxl2* in *N. furzeri*
foxl2-qRTR	GCTGTTCTGCCATCCCTTCT	
foxl3-qRTF1	GACCGGAAAAGCAACTTCTG	Quantification of *foxl2l* in *N. furzeri* trunks at 0 dph
foxl3-qRTR1	CGGTCATGTAAGGCACACTG	
foxl3-qRTF2	GATCCCGCATTTGAAGACAT	Quantification of *foxl2l* in adult *N. furzeri* gonads
foxl3-qRTR2	GGAGCCGCTCACATACTGAT	
Nf_Gdf6a_fw1	TTCCGCTCCTCTAAATCTGC	Quantification of *gdf6X* & *gdf6Y* in *N. furzeri* (Fig. 1E)
Nf_Gdf6a_rv1	TTCCTGAAAATCCGCAGTTC	
gdf6ex1qF1	CCATAACGAGTTTTGTGGACAGAGG	Quantification of *gdf6X* & *gdf6Y* in *N. furzeri* (Fig. S3A)
gdf6ex2qR1	CTGAAAATCCGCAGTTCCGC	
gdf6ex1qF1	CCATAACGAGTTTTGTGGACAGAGG	Quantification of *gdf6X* in *N. furzeri* (Fig. S3A; S6E)
Nf_Gdf6_rv4	GCGCTGCTGCTGATGATAGT	
gdf6ex1qF1	CCATAACGAGTTTTGTGGACAGAGG	Quantification of *gdf6Y* in *N. furzeri* (Fig. S3A; S6E)
Nf_Gdf6Y_rv4	GCGCTGCTGATGATGATGCC	
gdf6Y_3UTR_F1	ACTGAACGATTAATCCACCAGAC	Quantification of *gdf6Y* in *N. furzeri* (Fig. 1E)
gdf6/Y_3UTR_R11	ATAATAATGAACAGCAGTGCATTC	
KDM6B-F3	CAGACCACGCTACGGAAAAAG	Quantification of Nfu_g_1_015428 in *N. furzeri*
KDM6B-R23	CCTCCGCATCTGCCTCC	
LOC100572914-F6	AAGGACCATAGTGGCTGTCG	Quantification of Nfu_g_1_014802 in *N. furzeri*
LOC100572914-R5	CGAGGTCTTCACAGCACGTTT	
PCTPfw3	GGTAAACTGGGCAGCAAAGAG	Quantification of *pctp* in *N. furzeri*
PCTPrv3	GGTGGACACTTTCCCATCAG	
rec8F2	TTACCACCAGAGGCAAACCG	Quantification of *rec8* in *N. furzeri*
rec8R2	GATGTCTCCAAACGGCTCATG	
rnf19a_fwd1	TGGTGCCCATCTCTCTGTGT	Quantification of *rnf19a* in *N. furzeri*

rnf19a_rev1	TCTGCTACTGATGTCATGTCGG	
Sybu_fw1	CAACCCAGAGCAGTACCTGA	Quantification of all *sybu* transcript variants in *N. furzeri*
Sybu_rv1	TCTTCCCTCATTCTGCCAAG	
Sybu_fw7	AAGCTGCTGTGTGAAGCAGA	Quantification of *sybu* transcript variant 1 & 2 in *N. furzeri*
Sybu_rv2	CCTCTTCACTTTGGCTTTGC	
Sybu_fw9	GGAAGATCACTGAGTTTTGACC	Quantification of *sybu* transcript variant 3 in *N. furzeri*
Sybu_rv3	CAGGTACTGCTCTGGGTTGG	
TACC3_F2	ACCAACAGCTGAGCCCAAC	Quantification of *tacc3* in *N. furzeri*
TACC3_R2	TAGCTGCTGATCGGGCTG	
FIZ1-F3	CAGGACGATCACTCAGAACAAG	Quantification of *zfp2* in *N. furzeri*
FIZ1-R13	GCTCACTCTGCTCCTCTTC	
zfp36l2qRTF2	CGTCCAAACCGTGCTTCTTG	Quantification of *zfp36l2* in *N. furzeri*
zfp36l2qRTR2	TCTTTAGCGCACAGCTGGAA	
ZPC-F2	GACTGACCCCCGATCACAG	Quantification of *zp3* in *N. furzeri*
ZPC-R2	CTCATCTCCAGTAACCAGTTTCC	
ZPB_F	GGACCAAGAGGATCCATCAC	Quantification of *zp4* in *N. furzeri*
ZPB_R	CCCTGCAGCCGCCAC	
HsPUM1qRTF	TGCGGGAGATTGCTGGACAT	Quantification of *PUM1* as universal human reference gene (Rácz et al. 2021)
HsPUM1qRTR	GTGTGGCACGCTCCAGTTTC	
HsID1qRTF1	AGAACCGCAAGGTGAGCAAGG	Quantification of human *ID1*
HsID1qRTR1	AGGAACGCATGCCGCCTCG	
HsID2qRTF	CCTGCATCACCAGAGACCCG	Quantification of human *ID2*
HsID2qRTR	CAGAAGGGAATTCAGAAGCCTGC	
HsID3qRTF	CCTGACACCTCCAGAACGCA	Quantification of human *ID3*
HsID3qRTR	GAAGTTGGGGCCCATCCCTG	
HsLXNqRTF	GCCTGGGTTGCCTGTGGTTA	Quantification of human *LXN*
HsLXNqRTF	TGCCAGAGAACTTGCATTTGCC	
HsSMAD6qRTF	CGCGACGAGTACAAGCCACT	Quantification of human *SMAD6*
HsSMAD6qRTR	CGGAGACATGCTGGCGTCTG	
HsSMAD7qRTF	TGCAACCCCCATCACCTTAGC	Quantification of human *SMAD7*
HsSMAD7qRTR	CCCCCTGTTTCAGCGGAGGA	
HsZFP36L2qRTF	CAAGGGCTCCTCCCGACCTC	Quantification of human *ZFP36L2*
HsZFP36L2qRTR	CCAGGGATTTCTCTGTCTTGCAC	